Published in final edited form as:
J Am Chem Soc. 2023 December 06; 145(48): 26222–26237. doi:10.1021/jacs.3c08790.

Chemical Kinetic Method for Active-Site Quantification in Fe-N-C Catalysts and Correlation with Molecular Probe and Spectroscopic Site-Counting Methods

Jason S. Bates[a,*,‡], **Jesse J. Martinez**[a], **Melissa N. Hall**[a], **Abdulhadi A. Al-Omari**[b], **Eamonn Murphy**[c], **Yachao Zeng**[d], **Fang Luo**[e], **Mathias Primbs**[e], **Davide Menga**[f], **Nicolas Bibent**[g], **Moulay Tahar Sougrati**[g], **Friedrich E. Wagner**[h,†], **Plamen Atanassov**[c], **Gang Wu**[d], **Peter Strasser**[e], **Tim-Patrick Fellinger**[f,i], **Frédéric Jaouen**[g], **Thatcher W. Root**[b], **Shannon S. Stahl**[a,*]

[a]Department of Chemistry, University of Wisconsin–Madison, Madison, Wisconsin 53706, USA

[b]Department of Chemical and Biomolecular Engineering, University of Wisconsin–Madison, Madison, Wisconsin 53706, USA

[c]Department of Chemical and Biomolecular Engineering, National Fuel Cell Research Center, University of California, Irvine, California 92697, USA

[d]Department of Chemical and Biological Engineering, University at Buffalo, The State University of New York, Buffalo, New York 14260, USA

[e]The Electrochemical Catalysis, Energy and Materials Science Laboratory, Department of Chemistry, Technical University Berlin, 10623 Berlin, Germany

[f]Chair of Technical Electrochemistry, Department of Chemistry and Catalysis Research Center, Technische Universität München (TUM), 85748 Garching, Germany

[g]ICGM, Univ. Montpellier, CNRS, ENSCM, 34293 Montpellier, France

[h]Department of Physics, Technische Universität München (TUM), 85748 Garching, Germany

[i]Bundesanstalt für Materialforschung und -prüfung (BAM), 12203 Berlin, Germany

Abstract

Mononuclear Fe ions ligated by nitrogen (FeN_x) dispersed on nitrogen-doped carbon (Fe-N-C) serve as active centers for electrocatalytic O_2 reduction and thermocatalytic aerobic oxidations. Despite their promise as replacements for precious metals in a variety of practical applications, such as fuel cells, the discovery of new Fe-N-C catalysts has relied primarily on empirical approaches. In this context, the development of quantitative structure–reactivity relationships and

---

[*] **Corresponding Authors**: Shannon S. Stahl; stahl@chem.wisc.edu, Jason S. Bates; jsb9vw@virginia.edu.
[‡] Jason S. Bates: Department of Chemical Engineering, University of Virginia, Charlottesville, Virginia 22903, USA
[†] Deceased June 15, 2023.

Author Contributions
The manuscript was written through contributions of all authors. All Authors have given approval to the final version of the manuscript.

Supporting Information.
Additional experimental details, characterization data, kinetic data, and supplementary discussions are available in the Supporting Information document.

benchmarking of catalysts prepared by different synthetic routes and by different laboratories would be facilitated by the broader adoption of methods to quantify atomically dispersed FeN_x active centers. In the present study, we develop a kinetic probe reaction method that uses the aerobic oxidation of a model hydroquinone substrate to quantify the density of FeN_x centers in Fe-N-C catalysts. The kinetic method is compared with low-temperature Mössbauer spectroscopy, CO pulse chemisorption, and electrochemical reductive stripping of NO derived from NO_2^- on a suite of Fe-N-C catalysts prepared by diverse routes and featuring either the exclusive presence of Fe as FeN_x sites or the coexistence of aggregated Fe species in addition to FeN_x. The FeN_x site densities derived from the kinetic method correlate well with those obtained from CO pulse chemisorption and Mössbauer spectroscopy. The broad survey of Fe-N-C materials also reveals the presence of outliers and challenges associated with each site quantification approach. The kinetic method developed here does not require pretreatments that may alter active-site distributions nor specialized equipment beyond reaction vessels and analytical instrumentation (e.g., NMR).

Graphical Abstract

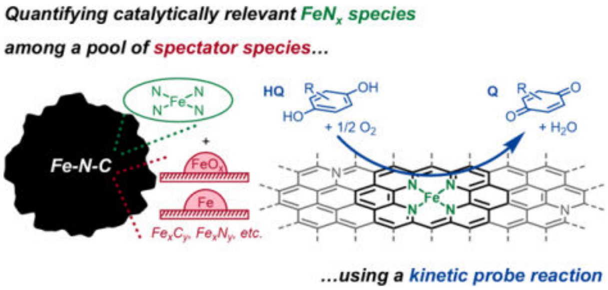

Introduction

Catalysts consisting of iron incorporated into nitrogen-doped carbon (Fe-N-C) are leading alternatives to precious metal electrocatalysts for the O_2 reduction reaction (ORR) in fuel cells,[1–4] and they are increasingly being used for the thermochemical aerobic oxidation of organic molecules.[5–7] Mononuclear Fe species ligated at nitrogen-containing defects (FeN_x) are widely recognized as the active centers for ORR [8 – 10] electrocatalysis and the aerobic oxidation of alcohols[11,12] and hydroquinones.[13] However, the high-temperature pyrolysis methods that are typically used to synthesize Fe-N-C catalysts often form Fe aggregates and carbon structures that bury FeN_x centers in locations that are inaccessible to reacting molecules (Figure 1A).[7] Such active-site diversity is common in heterogeneous catalysts and highlights the need for accurate quantification of the density of accessible FeN_x species (i.e., the number of sites per catalyst mass), particularly when they are present within a mixture of other Fe-based species. The accurate measurement of the site density of catalytically relevant FeN_x centers enables assessing the intrinsic reactivity of the FeN_x centers, i.e., their turnover frequencies (TOF), in critical and emerging applications. TOF measurements, in turn, facilitate the comparison, benchmarking, and reproducibility of catalysts synthesized by different routes and by different researchers.[14–17] While the accuracy of methods used to assess FeN_x site densities is still debated, [18–20] these methods are being to be used to guide synthetic design of Fe-N-C electrocatalysts.[21–23] In contrast, similar methods have seldom been applied to the study or development of Fe-N-C catalysts used in thermal catalytic applications.[7] The work presented herein bridges these different fields and provides a foundation for characterization of catalysts use in either electrochemical or thermal applications.

Widely adopted strategies to quantify FeN_x site densities in Fe-N-C catalysts consist of spectroscopic methods or chemical titrations with probe molecules. ^{57}Fe Mössbauer spectroscopy is a bulk method that detects all Fe species in a material and distinguishes between them based on their hyperfine parameters. These spectroscopic fingerprints identify the phases of Fe aggregates[24–26] and distinguish mononuclear species with different oxidation states from one another,[27] and their peak areas can be interpreted quantitatively at low temperatures (4–10 K).[28] Low temperatures are also necessary to identify the presence of superparamagnetic Fe species.[26, 29] Dodelet and coworkers showed that the ORR reactivity of five Fe-N-C catalysts correlates poorly with the room-temperature Mössbauer peak area of a mononuclear species, although the linearity of the correlation is improved when weighted by the BET surface area of each catalyst.[30] Thus, while Mössbauer spectroscopy provides clear insights into Fe speciation in a material, it does not provide direct information about the accessibility of the different Fe centers.[7,18] *In situ* approaches that combine a catalytic stimulus or the adsorption of a probe molecule with Mössbauer spectroscopy show promise,[10,31,32] but they have not yet been applied in the context of active-site quantification.

Chemical titrations rely on the selective binding of a molecular probe to FeN_x sites with a known stoichiometry so that their adsorbed quantity can be directly related to the FeN_x site density. Reported titrants for FeN_x species include CO,[33] NO,[34] and CN^-[35] (Figure 1B). In each case, specific conditions are required for titrant exposure and catalyst pretreatment to ensure that the saturation coverage of the titrant on FeN_x centers is accurately quantified.

CO pulse chemisorption (Figure 1B-i) quantifies the adsorption of gas-phase CO to FeN_x centers at 193 K.[33] Subambient temperatures are needed because CO adsorbs weakly to FeN_x centers and begins to desorb at ~260 K.[33] Strasser and coworkers have shown that a pretreatment at 873 K is required to ensure that oxygenated species adsorbed to FeN_x centers under ambient conditions are desorbed, leaving FeN_x vacant and able to bind CO.[36] The FeN_x site density determined by CO pulse chemisorption has been found to correlate well with the ORR reactivity of a series of Fe-N-C catalysts synthesized using polyaniline combined with other N-containing additives as nitrogen sources.[37]

Nitrosyl species bound to FeN_x centers can be quantified by electrochemical reductive stripping in acidic aqueous electrolyte (Figure 1B-ii).[34] Quantitative formation of $NO–FeN_x$ species occurs at open-circuit potentials after saturation with NO_2^- under neutral aqueous conditions, followed by exposure to acidic aqueous conditions to convert NO_2^- to NO according to the equation: $NO_2^-–FeN_x + H^+ \rightarrow NO–FeN_x + H_2O$.[34,38] Prior to the formation and quantification of $NO–FeN_x$ species, Fe-N-C catalysts are bound to an electrode within a Nafion film and undergo extensive redox cycling in acidic aqueous electrolyte.[34,39]

CN^- titration occurs in a divided electrochemical cell with a graphite working electrode containing a stirred slurry of Fe-N-C in an Ar-purged acidic aqueous electrolyte (Figure 1B-iii).[35] The measured uptake of CN^- is correlated with the fractional decrease of the ORR current (0.85 V_{RHE}, 0.1 M $HClO_4$ electrolyte) relative to a pristine Fe-N-C catalyst and extrapolated to the CN^- uptake where the ORR current becomes zero, reflecting the saturation of FeN_x with CN^-. To ensure irreversible CN^- adsorption, O_2 is purged from the cell under flowing Ar and the cell is polarized at 0.5 V_{RHE} to strip oxygen-derived species from Fe-N-C. The cell is then stabilized at 1.0 V_{RHE} before CN^- is added at this condition.

Comparative studies of the approaches described above are limited,[7,18,35] but those that are available highlight drawbacks associated with each technique. A cross-laboratory study comparing CO pulse chemisorption and NO stripping observed that NO quantified 12–39% of the sites quantified by CO on a series of four Fe-N-C catalysts. This discrepancy was ascribed to different accessibility of active centers for the two techniques.[18] For example, the high-temperature pretreatment used before CO pulse chemisorption may redisperse aggregated species to atomically dispersed species,[40] and a gas-phase titrant may not access the same number of active centers as liquid-phase catalytic reactions. The 1:1 binding stoichiometry of CO to FeN_x also remains an assumption. On the other hand, the Nafion film configuration used for NO stripping may alter the accessibility of FeN_x binding sites, and the redox cycling pretreatment that is used may influence their distribution. Additionally, converting the stripping charge to a quantity of NO–FeN_x species requires assignment of a specific reduction product, and both 5 e^- (NH_4^+)[34] and 3 e^- (NH_2OH)[41] products have been proposed. Bae et al. quantified the same number of active centers on one Fe-N-C catalyst regardless of whether CO, NO (assuming 3 e^- reduction of NO), or CN^- was used,[35] but the generality of this observation for other catalysts was not probed.

Methods that expand beyond probe molecules and spectroscopy have also been developed. Fellinger and coworkers circumvented the challenges associated with probe molecules by synthesizing an Fe-N-C catalyst containing predominantly FeN_x centers, then systematically leached Fe from the material to generate a series of three catalysts with varying FeN_x contents that correlated linearly with their ORR current density (0.70–0.80 V_{RHE}, 0.1 M $HClO_4$).[42] While this strategy was effective for determining the ORR turnover frequency of the active centers in a model material, the extension of this approach to materials that possess a mixture of active site structures has not yet been demonstrated. In another approach, Elbaz and coworkers applied Fourier-transform alternating current voltammetry to quantify the charge putatively associated with the $Fe^{II/III}N_x$ redox transition.[43] This technique was applied to two commercially available Fe-N-C catalysts and estimated ~60% of the active-site density quantified by NO stripping.[43] Lastly, Yu and coworkers have employed scanning electrochemical microscopy in combination with redox probes to quantify FeN_x centers,[44,45] but this strategy has not been adopted by other groups to date. The different conditions and disagreement among active-site quantification techniques, together with the specialized equipment and/or experimental challenges associated with certain techniques, motivate the development of other methods that could aid in the comparison of Fe-N-C catalysts prepared by different synthetic routes and by different research groups.

Here, we develop a new kinetic approach to quantify FeN_x centers (exemplarily illustrated as planar tetrapyridinic FeN_4 sites in Figure 1C) and compare it directly with low-temperature ^{57}Fe Mössbauer spectroscopy, CO pulse chemisorption, and reductive stripping of NO derived from NO_2^-. This kinetic approach relies on quantifying the initial rate of hydroquinone (HQ) oxidation to a quinone by aerobic oxidation in an aqueous slurry-phase semibatch reactor. The method uses an easily synthesized water-soluble, quinone derivative[46,47] and requires no pretreatments to the Fe-N-C catalyst. The initial rate reflects surface reactions at FeN_x centers but not at Fe aggregates, as shown by our previous work.[13,48] The synthesis of Fe-N-C catalysts containing FeN_x sites on solvent-accessible surfaces using recently developed approaches[13,49] therefore enables estimation of the intrinsic turnover frequency (TOF) of HQ oxidation. The HQ oxidation TOF, in turn, permits calculation of the FeN_x site density on any material solely from its initial HQ oxidation rate. This kinetically quantified FeN_x site density correlates well with values obtained from CO pulse chemisorption and Mössbauer spectroscopy for a suite of Fe-N-C catalysts with diverse synthetic origins, bulk Fe contents, and Fe speciation. The straightforward nature of this approach should make it a compelling complement to existing site-quantification methods.

Results and Discussion

Assessing the Intrinsic Reactivity of FeN_x Centers in Fe-N-C Catalysts.

Fe-N-C catalysts containing predominantly FeN_x centers at solvent-accessible surfaces were synthesized to quantify the intrinsic reactivity of FeN_x centers. Fe-N-C catalysts with these attributes can be synthesized via recently reported strategies to metalate vacant macrocyclic N_x binding sites on nitrogen-doped carbon scaffolds (Figure 2A).[13,49,50] A metal–organic framework composed of Zn^{2+} nodes with imidazolate linkers, ZIF-8, was synthesized by reported methods[51] and used as the precursor for the N-doped carbon. ZIF-8 was treated under flowing N_2 at 1323 K to yield a nitrogen-doped carbon material containing both ZnN_x centers and vacant N_x binding sites.[13,52] This material was contacted with a solution of $FeCl_2$ in DMF at 423 K under N_2 to effect the metalation of vacant N_x centers with Fe (Figure 2A). The use of solution-phase conditions ensures that Fe species are deposited on solvent-accessible surfaces of the material. Two different concentrations of Fe were used to synthesize two materials with different bulk Fe contents (0.1 wt% and 0.4 wt%). After metalation treatments, washing, and recovery of the solids, the materials were treated under flowing N_2 at 873 K for 2 h in order to ensure the complete dispersion of Fe species,[13] and to facilitate comparisons of reactivity with CO pulse chemisorption measurements that require a pretreatment under the same conditions.[36] The two catalysts synthesized by the metalation of ZIF8-derived nitrogen-doped carbon are referred to as xFe-N-$C^{m\text{-}ht}$, where x refers to the Fe wt% quantified by ICP-OES, and "m-ht" indicates that metalation followed by a heat treatment was the synthetic route.

The Fe speciation of the two catalysts was characterized by low-temperature Mössbauer spectroscopy (10 K). The Mössbauer spectra (Figure 2B) are predominantly composed of a single doublet component referred to as "D1," which is assigned to a mononuclear $Fe^{III}N_x$ species.[27] Other minor components include "D2," which is assigned to an $Fe^{II}N_x$

species,[27] “D3,” a high-spin Fe^{II} species that corresponds to $FeCl_2 \cdot 4H_2O$ remaining from the synthesis,[52] and a sextet assigned to FeO_x aggregates (see section 3.1 and Figures S1 and S2 in the Supporting Information for additional discussion of fitting and parameters). The relative peak areas of each component in Mössbauer spectra can be interpreted to quantify the relative molar fraction of bulk Fe in the material when the Lamb–Mössbauer factors of all species are equivalent. Sougrati et al. showed that this is a reasonable assumption for D1, D2, α-Fe, and γ-Fe species only at low temperatures (5–10 K).[28] With this assumption, the FeN_x active-site density can be calculated according to eq 1:

$$N_{FeN_x,\,Möss} = N_{Fe,\,bulk} \times \frac{A\%_{D1}}{100} \tag{1}$$

where $N_{Fe,bulk}$ (mol g^{-1}) is the total Fe content quantified by ICP-OES, and $A\%_{D1.}$ reflects the percentage of total area assigned to D1 in the Mössbauer spectrum. Applying this analysis to the two Fe-N-C$^{\text{m-ht}}$ materials gives active-site densities of 19 ± 9 μmol g^{-1} and 48 ± 11 μmol g^{-1}, where the standard errors result from least-squares fitting of the Mössbauer spectra. Similar analysis, accounting for the area of D1+D2 Fe sites, is presented in section 6 of the Supporting Information. We assume that all FeN_x species assigned as active sites by Mössbauer spectroscopy in the Fe-N-C$^{\text{m-ht}}$ materials reside in pore environments that are accessible to the DMF-solvated $FeCl_2$ precursor used for metalation. These quantitative active-site densities facilitate direct correlations with catalytic reactivity.

The aerobic oxidation of a sulfonated hydroquinone (Figure 2C) was chosen as a catalytic probe reaction. This reaction was chosen because it is mechanistically well-understood and rates can be measured under kinetically limiting conditions[48] and because it is catalyzed by FeN_x centers.[13] Additional discussion of transport limitations can be found in section 4.2 of the Supporting Information. The conditions of the measurement shown in Figure 2C define initial reaction rates that reflect the quasi-equilibrated adsorption of O_2 at FeN_x sites followed by kinetically relevant hydrogen-atom transfer from a physisorbed HQ molecule present on the doped carbon surface at saturation coverages.[48] The initial rate of HQ oxidation (per g$_{\text{catalyst}}$) was measured in semibatch reactors on Fe-N-C$^{\text{m-ht}}$ catalysts and their N-C precursor. The rate on the nominally Fe-free N-C precursor was 11–24% of the rate catalyzed by the Fe-N-C$^{\text{m-ht}}$ catalysts and was subtracted from these rates to give the rate catalyzed by FeN_x sites. These corrected HQ oxidation rates correlate linearly with the FeN_x active-site density of the Fe-N-C$^{\text{m-ht}}$ catalysts (Figure 2D, solid line), according to eq 2:

$$r_{HQ,\,corr} = r_{HQ,\,Fe-N-C} - r_{HQ,\,N-C} = TOF_{FeN_x} \times N_{FeN_x,\,Möss} \tag{2}$$

where $r_{HQ,Fe\text{–}N\text{–}C}$ (mol g^{-1} s^{-1}) is the HQ oxidation rate measured on the Fe-N-C catalyst, $r_{HQ,N\text{–}C}$ (mol g^{-1} s^{-1}) is the HQ oxidation rate measured on the N-C precursor, $r_{HQ,corr}$ (mol g^{-1} s^{-1}) represents the corrected HQ oxidation rate attributed to Fe species, and $TOF_{FeN_x}\left(s^{-1}\right)$ is the turnover frequency of HQ oxidation catalyzed by FeN_x sites. The value of TOF_{FeNx}, 1.1 ± 0.3 s^{-1}, reflects the intrinsic reactivity of the surface FeN_x sites in these two Fe-N-C$^{\text{m-ht}}$ catalysts.

The definition of TOF_{FeNx} provides an opportunity to interrogate the behavior of Fe-N-C catalysts that contain a mixture of Fe species. In these cases, the HQ oxidation rate could reflect contributions from these other species, e.g., FeO_x and γ-Fe aggregates, reflected by eq 3:

$$r_{HQ,\,corr} = TOF_{FeN_x} \times N_{FeN_x} + TOF_{FeO_x} \times N_{FeO_x} + TOF_{\gamma-\mathrm{Fe}} \times N_{\gamma-\mathrm{Fe}} + \cdots \quad (3)$$

where TOF_i: (s^{-1}) and N_i (mol g^{-1}) reflect the turnover frequency and surface site density of any species *i*. In the limiting case where TOF_{FeNx} is much larger than the TOF of any other species, the HQ oxidation rate can be used to calculate the FeN_x site density on any Fe-N-C material according to eq 4:

$$N_{FeN_x,\,HQ} = r_{HQ,\,corr}/TOF_{FeN_x} \quad (4)$$

FeO_x species[10,53] and Fe/Fe_3C species[54] show low ORR reactivity on their own, especially in acidic medium, and our prior study showed that the coexistence of aggregated Fe species with FeN_x species on Fe-N-C catalysts leads to a lower HQ oxidation rate (per total Fe) than on Fe-N-C catalysts containing only FeN_x species.[13] These observations are consistent with the assumptions that lead to eq 4. We will further probe these assumptions by comparing FeN_x site densities calculated using eq 4 with alternative active-site quantification methods based on molecular probes. This approach begins with 0.4Fe-N-$C^{m\text{-}ht}$ as an example.

Quantification of FeN_x Active Sites in Fe-N-C Catalysts using Molecular Probes.

The methods of CO pulse chemisorption and electrochemical stripping of NO derived from NO_2^- were used to obtain independent estimates of the FeN_x active-site density of 0.4Fe-N-$C^{m\text{-}ht}$. CO pulse chemisorption was performed in a gas-phase flow-through setup at 195 K after a pretreatment at 873 K in flowing He (Figure 3A), as previously reported.[36] Reduced CO peak areas (m/z = 28 detected by mass spectrometry) in the first two pulses reflect CO adsorption to FeN_x centers with a cumulative uptake of 46 μmol g^{-1}, while equal peak areas observed for the third through tenth pulses indicate saturation of the FeN_x sites (Figure 3A). A control experiment with the ZIF-8-C material prior to metalation shows only 3 μmol g^{-1} uptake (Figure S12, Supporting Information), confirming that FeN_x centers adsorb CO in 0.4Fe-N-$C^{m\text{-}ht}$. We consider this uptake (3 μmol g^{-1}) to be the minimum error associated with the CO pulse chemisorption measurement.

The electrochemical stripping of NO derived from NO_2^- was measured on a Nafion-bound film of 0.4Fe-N-$C^{m\text{-}ht}$ deposited onto a rotating-disc electrode following protocols adapted from Kucernak and coworkers.[34,39,55] The material was exposed to a 0.125 M NO_2^- solution and then the adsorbed NO_2^- was converted to NO by exposure to H^+ in a buffered electrolyte solution (0.5 M acetate, pH = 5.2, Figure 3B). The electrochemical ORR kinetic current density (0.8 V_{RHE}) decreased by a factor of 12 after NO poisoning (Figure S28b, Supporting Information), which is consistent with adsorption of NO to FeN_x active centers, rendering them inactive. The adsorbed NO was electrochemically stripped from FeN_x centers by executing a cyclic voltammetry scan between 0.4 V_{RHE} and −0.3 V_{RHE} under Ar. The baseline current density measured under the same CV conditions prior to the measurement of ORR reactivity (blue curve, Figure 3B) was subtracted from a stripping CV measured following NO poisoning (red curve, Figure 3B) to yield the stripping current density associated with NO–FeN_x species (black curve, Figure 3B). The accuracy of this measurement is highly sensitive to the reproducibility of the baseline CV scan. A reliable baseline is essential to ensure that the stripping charge reflects only NO stripping and not currents associated with capacitance changes or other redox events in the film. It can be observed that the green CV in Figure 3B labeled “Recovered”, collected following NO stripping, does not match the blue “Unpoisoned” CV. Through control experiments measuring the CVs of films lacking FeN_x centers such as those containing carbon black and ZIF-8-C, we concluded that such confounding factors were causing the “Recovered” CV to be poorly reproducible, so we chose to use the “Unpoisoned” CV as the reference to calculate the NO stripping current density. Further discussion of these challenges and comparisons of alternative baseline and stripping CV calculations can be found in section 3.3 of the Supporting Information. The integration baseline shown in orange in Figure 3B was shifted vertically in the analysis with the intent to correct for baseline differences that persisted between the stripping and unpoisoned CVs. This baseline shift was not required for all materials investigated in this work but was required in this case, further illustrating the challenges associated with the NO stripping method. The integrated stripping charge of 7.3 C g^{-1} is converted to a molar quantity of 25 μmol g^{-1} NO by assuming that the NO reacts with 3 H^+ and 3 e^- to form NH_2OH as reported previously[35,41] (site density values assuming 5 e^- to form NH_4^+ are reported in Table S3 in the Supporting Information). The NO reduction stoichiometry/product identity adds one additional complicating feature of this measurement.

The FeN_x site densities quantified by CO and NO titrations are compared in Figure 3C with those derived from HQ oxidation and Mössbauer spectroscopy. The HQ-based site density calculated by eq 4 uses the value of TOF_{FeNx} estimated in Figure 2C, and thus agrees with the Mössbauer site density by definition; however, this relationship will not be guaranteed for catalysts made by alternative synthetic routes (*vide infra*). The FeN_x site density quantified by CO closely agrees with that estimated by the HQ and Mössbauer methods, whereas NO quantifies a lower FeN_x site density (52–55% of the other methods). Lower active-site densities quantified by NO are consistent with a previous cross-laboratory study,[18] and these differences may have chemical or procedural origins. Chemically, (i) there may be reduced active-site accessibility in the ionomer-containing film used to contact the catalyst with an electrode, or (ii) FeN_x active centers may degrade during the extensive redox cycling pretreatments used before NO stripping. Procedurally, key assumptions may not be met, including (i) that the baseline used to correct the stripping data accurately leads to the quantification of NO stripping charge and no other spurious contributions, and (ii) that the stripping event reflects a well-defined stoichiometric reduction event to NH_2OH (or NH_4^+) rather than a mixture of products. Next, we extend these comparisons to include a suite of Fe-N-C catalysts synthesized by diverse routes and containing different distributions of $Fe^{II}N_x$ and $Fe^{III}N_x$ species in addition to different proportions of FeN_x sites coexisting with a variety of aggregated Fe species.

Quantification of FeN_x Active Sites in Fe-N-C Catalysts Synthesized by Diverse Methods.

Twelve additional Fe-N-C catalysts were synthesized by different routes by six different laboratories and acquired from one fuel cell catalyst company to supplement the Fe-N-$C^{m\text{-}ht}$ catalysts described above (Table 1). Fe-N-C materials are generally named "*x*Fe-N-C[descriptor]", where the leading *x* denotes the bulk Fe content quantified by ICP-OES. [56] Adventitious air was included in solution-phase metalation treatments to intentionally deposit FeO_x species alongside FeN_x species in *x*Fe-N-$C^{ma\text{-}ht}$ materials ("ma" = metalation with air). A 0.3Fe-N-$C^{HCl\text{-}m\text{-}ht}$ material was synthesized by the solution-phase metalation (cf. Figure 2A) of HCl-treated ZIF-8-derived carbon. Another Fe-N-C material was synthesized by a $FeCl_3$/LiCl eutectic salt melt metalation of a Zn-N-C material prepared via salt templating pyrolysis of 1,2-dicyanobenzene within a $ZnCl_2$/LiCl mixture, followed by HCl washing and flash pyrolysis, and is denoted 4.7Fe-N-C-ST, where "ST" reflects the salt templating procedure used by the team at BAM (Bundesanstalt für Materialforschung und -prüfung). [57] A 1.5Fe-Phen-C catalyst was synthesized by the pyrolysis of a carbon-supported $[Fe(Phen)_3]^{2+}$ complex. A 1.2Fe-PANI-C catalyst was synthesized by the pyrolysis of a carbon-supported Fe/polyaniline mixture. A second catalyst was synthesized by the pyrolysis of a mixture of activated carbon support, Fe precursor, and polyaniline, and is denoted 5.7Fe-N-C-TUB (TUB = Technical University Berlin).[58] A 0.5Fe-N-C-UCI catalyst (UCI = University of California, Irvine) was synthesized by the impregnation of an Fe/nicarbazin mixture into a sacrificial nanoporous silica template via pyrolysis and acid etching.[59,60] A commercial fuel cell catalyst was obtained from Pajarito Powder, denoted 0.5Fe-N-C-PAJ.[61] Two *x*Fe-N-C-UB catalysts were prepared by the pyrolysis of an Fe_2O_3@ZIF-8 composite under different gas compositions, namely 10% H_2/Ar (0.9Fe-N-C-UB; UB = University at Buffalo) and Ar (0.8Fe-N-C-UB). [62] A 0.8Fe-N-C-CNRS catalyst was synthesized by the pyrolysis of a ball-milled mixture of ZIF-8, $Fe(OAc)_2$, and 1,10-phenanthroline under Ar at 1323 K (CNRS = Centre National de la Recherche Scientifique).[8]

The FeN_x active-site density of all fourteen Fe-N-C catalysts ($N_{FeNx,HQ}$) was estimated using the kinetic HQ oxidation approach and compared with alternative quantification approaches. CO pulse chemisorption data ($N_{FeNx,CO}$) were measured on thirteen catalysts, NO stripping profiles ($N_{FeNx,NO}$) were measured on thirteen catalysts, and Mössbauer spectra ($N_{FeNx,Möss}$) were measured on eleven catalysts. These site densities are compared for each catalyst in Figure 4A. In a few cases, there was not sufficient material to employ all four characterization methods. We note that although the value of $N_{FeNx,Möss}$ is determined using the area of the D1 component according to eq 1, we have also included a full analysis with D1+D2 in Section 6 of the Supporting Information. We will focus on each materials class in turn, then assess broader trends in the comparison between active-site quantification approaches.

Fe-N-C catalysts derived from solution-phase metalation approaches (black squares and circles, Figure 4A) and a eutectic salt melt metalation strategy (4.7Fe-N-C-ST, yellow pentagon, Figure 4A) generally show agreement between $N_{FeNx,HQ}$ and $N_{FeNx,CO}$. NO stripping quantified fewer FeN_x sites than HQ and CO in several cases. Mössbauer spectroscopy shows wider but nonsystematic variations: in the case of 8.4Fe-N-$C^{ma\text{-}ht}$,

$N_{FeNx,Möss}$ is smaller than the values given by the other methods (44–83%); and in the case of 1.3Fe-N-C$^{ma\text{-}ht}$, $N_{FeNx,Möss}$ is higher by a factor of 1.7–2.4. The Mössbauer spectrum of 8.4Fe-N-C$^{ma\text{-}ht}$ (Figure S4) shows that the majority of Fe is present as FeO_x (97 ± 6%), which leads to a large error in the deconvoluted area that reflects the FeN_x site fraction (3 ± 3%). The Mössbauer spectrum of 1.3Fe-N-C$^{ma\text{-}ht}$ shows that over 50% of the Fe in the material is present as FeO_x (Figure S3), but the D1 doublet feature assigned to $Fe^{III}N_x$ is not subject to large fitting errors (32 ± 3%). However, the presence of magnetically ordered FeO_x aggregates in this material suggests that there might also be nanosized FeO_x aggregates, which can behave as superparamagnetic species even at 10 K and lower.[26,63–65] Such species show a D1-like signal rather than a sextet feature, causing the FeN_x site density by eq 1 to be overestimated. These cases illustrate two drawbacks of Mössbauer spectroscopy: (i) its accuracy becomes poor when FeN_x is a minority species in the spectrum, and (ii) small FeO_x aggregates may contribute to D1 peak area identified as FeN_x species. In contrast, CO chemisorption has been shown to be insensitive to FeO_x sites,[19,33,36,37] and the HQ and CO methods give site densities within reasonable agreement for these materials. This similarity between FeN_x site densities quantified by HQ oxidation and CO pulse chemisorption suggests that FeO_x sites that coexist with FeN_x centers do not contribute significantly to HQ oxidation.

Close agreement between $N_{FeNx,HQ}$ and $N_{FeNx,CO}$ is also observed for materials prepared by pyrolysis of material containing a molecular Fe complex (1.5Fe-Phen-C, open circle in Figure 4A) and from an Fe/polyaniline/carbon mixture (1.2Fe-PANI-C and 5.7Fe-N-C-TUB, open circle and blue triangle in Figure 4A, respectively). The Mössbauer spectra of these materials show peaks for metallic and carbidic Fe, and in the case of the PANI-derived materials, Fe_3S_4 (Figure S6–S8). The values of $N_{FeNx,NO}$ for these materials deviate from $N_{FeNx,HQ}$ and $N_{FeNx,CO}$ by factors of 0.5–1.8, without a systematic deviation. Mössbauer spectroscopy agrees well with the other methods in the case of 1.5Fe-Phen-C, but it estimates a higher FeN_x site density than the other methods when applied to the polyaniline-derived catalysts. The value of $N_{FeNx,Möss}$ is higher than $N_{FeNx,HQ}$ by a factor of 2 for 1.2Fe-PANI-C and by a factor of 3.7 for 5.7Fe-N-C-TUB. The Mössbauer spectrum (Figure S8) of 5.7Fe-N-C-TUB is broader than those measured on other materials and shows a minority of D1 species, resulting in a larger error (12 ± 12% D1). So, subsequent analyses will be considered both with and without this outlier. The close agreement between HQ and CO in these cases is consistent with their selectivity for FeN_x quantification, without interference from Fe metal, carbide, and sulfide particles.

The 0.5Fe-N-C-UCI and 0.5Fe-N-C-PAJ materials are synthesized via a similar silica-templating approach.[66,67] The FeN_x active-site densities of 0.5Fe-N-C-PAJ (red star, Figure 4A) quantified by all four approaches are similar, within error, whereas the kinetic method quantified higher active-site densities than CO and NO on 0.5Fe-N-C-UCI (green diamond, Figure 4A). Potential reasons for this disagreement include (1) that the intrinsic reactivity of some FeN_x centers is higher in 0.5Fe-N-C-UCI than in the metalated materials used to determine TOF_{FeNx}, (2) that FeN_x centers become occluded or degraded by pretreatments prior to probe-molecule measurements (873 K for CO, redox cycling for NO), or (3) that probe molecules do not saturate all FeN_x centers under the conditions of the measurement.

The *x*Fe-N-C-UB and 0.8Fe-N-C-CNRS catalysts were synthesized by variations on an approach based on the pyrolysis of the ZIF-8 metal–organic framework. The 0.8Fe-N-C-CNRS catalyst (orange circle, Figure 4A) shows good agreement between active-site densities quantified by HQ, CO, and Mössbauer, but not NO. In contrast, the values of $N_{FeNx,HQ}$ are higher than $N_{FeNx,CO}$ by factors of 1.6–2.0 on *x*Fe-N-C-UB catalysts (blue squares, Figure 4A). Further, the value of $N_{FeNx,NO}$ matches $N_{FeNx,CO}$ in one case (0.8Fe-N-C-UB) but is significantly lower in the other case (0.9Fe-N-C-UB). The Mössbauer spectrum (Figure S10, Supporting Information) of 0.8Fe-N-C-UB estimates an FeN_x active-site density that lies between those of the kinetic and probe-molecule methods. Among these Fe-N-C materials, NO consistently estimates a lower FeN_x active-site density than the other methods as observed in other studies.[19] Potential reasons for these deviations have been discussed above, and one additional reason could be that accurate estimates for the Fe-free N-C HQ oxidation rate were not available on these materials, which would lead to an overestimate of the active-site density by HQ oxidation (cf. eq 2 and eq 4, where $r_{HQ,N-C} = 0$).

The FeN_x active-site density can also be expressed as an Fe utilization after normalization to the total bulk Fe content in each material.[33] The Fe utilization value is crucial to assess the reasonableness of an active-site quantity, as values >1 likely suggest problems with the measurement or underlying assumptions of the method. All Fe utilization values shown in Figure 4B fall between 0–1, indicating that Fe is a reasonable source of all of the sites counted by the protocols used in this study. Kucernak and coworkers have shown that gas-phase NO also adsorbs at sites not associated with Fe on Fe-N-C surfaces,[68] consistent with another report where gas-phase NO exposure estimated a ~2× higher site density than NO derived from NO_2^- exposure.[52] In fact, Fe utilization values >1 and as high as 6 have gone unnoticed in NO titration data.[69–71] These considerations highlight how Fe utilization should serve as a first diagnostic for unselective titration or other methodological artifacts.

Comparison of FeN_x Active-Site Quantification Methods.

Correlations between $N_{FeNx,HQ}$ and each of the other three active-site quantification methods are shown as parity plots in Figure 5. The remaining correlations between the other methods can be found in Figure S48 of the Supporting Information. The deviation from parity is assessed as the mean absolute error (MAE) and the mean percentage error (MPE), where smaller values indicate better agreement between the two active-site quantification methods (for more details, see section 5 of the Supporting Information). Data points that lie in the lower-right of the parity plots indicate overcounting by HQ and/or undercounting by the other method, whereas data points in the upper-left reflect the inverse.

The strongest correlation between two FeN_x active-site quantification methods is observed with the HQ oxidation and CO pulse chemisorption techniques (Figure 5A, MAE = 1.4, MPE = 26%). The correlation between HQ and NO is rather poor (Figure 5B, MAE = 2.3, MPE = 53%). Mössbauer spectroscopy also shows worse agreement with HQ oxidation than does the CO pulse chemisorption technique (Figure 5C, MAE = 2.1, MPE = 38%), even after removal of the 5.7Fe-N-C-TUB outlier (MAE = 1.6, MPE = 32% after removal of 5.7Fe-N-C-TUB). Three outliers in Figure 5A fall in the lower-right of the parity plot because CO may undercount or because HQ oxidation may overcount active sites, whereas the inverse is the case for 4.7Fe-N-C-ST (yellow pentagon). NO generally estimates fewer FeN_x active-sites than HQ or CO (Figure 5B and S48A), which is consistent with prior reports[18] and inconsistent with the hypothesis that NO adsorbs to Fe aggregates.[53] The poor NO correlation may be due, in part, to challenges in obtaining a reproducible baseline as discussed in section 3.3.2 of the Supporting Information. The correlation between Mössbauer spectroscopy and HQ oxidation in Figure 5C does not show systematic outliers.[72] The major outlier, 5.7Fe-N-C-TUB, and the two data points that are the next-farthest from parity (xFe-N-$C^{ma\text{-}ht}$, black circles) illustrate two major challenges with Mössbauer spectroscopy, which were noted above: (i) that large errors result when FeN_x centers are a minority species (<10% in 8.4Fe-N-$C^{ma\text{-}ht}$, Figure S4) which causes the data point to appear in the lower right of Figure 5C, and (ii) that sufficiently small FeO_x clusters may not become magnetically split into a sextet feature and would be misidentified as FeN_x species (as in 1.3Fe-N-$C^{ma\text{-}ht}$, Figure S3 and 5.7Fe-N-C-TUB, Figure S8), causing the data points to appear in the upper left of Figure 5C. These quantitative comparisons based on a suite of Fe-N-C catalysts indicate that the kinetic active-site quantification strategy developed here correlates well with CO pulse chemisorption and, in most cases, with Mössbauer spectroscopy.

Each FeN_x active-site quantification technique can be further compared on several qualitative bases: the conditions of the measurement, the fundamental and practical challenges that these conditions engender, and the generality of the method for other MN_x sites (M ≠ Fe), as summarized in Table 2. The fundamental limitations have been described in detail in the foregoing discussion and are summarized as follows: (i) some methods may not accurately differentiate FeN_x from other Fe species in some cases (Mössbauer), (ii) pretreatment and measurement conditions can cause active-site distributions to change (CO, NO), (iii) errors can arise associated with materials limitations such as low FeN_x fraction (Mössbauer) or lack of data on an Fe-free analog (HQ), and (iv) inaccuracies due to unexpected deviations from fundamental assumptions such as active-site saturation (CO, NO) or intrinsic reactivity of sites (HQ). The methods included in Table 2 alongside HQ oxidation were selected based on their reported ability to quantitatively distinguish accessible FeN_x sites and their breadth of adoption in the field. Other characterization techniques, such as X-ray absorption spectroscopy, are commonly used, but they lack the ability to accurately quantify FeN_x in the presence of Fe species and to distinguish accessible from inaccessible sites, and are therefore not included.[7,73,74]

Practical limitations are also important to consider for adoption of these methods. Mössbauer spectroscopy and CO pulse chemisorption require costly spectroscopic or gas-phase analytical instrumentation, whereas NO electrochemical stripping and HQ oxidation use comparatively simple equipment. This study shows that no single active-site quantification technique should be employed on its own, but rather at least two should be compared and validated for accurate comparison of catalysts with one another. The inclusion of HQ oxidation kinetics as a new method should facilitate active-site quantification by laboratories lacking specialized materials characterization equipment. HQ oxidation also provides a rapid screening approach to down-select materials for more costly or time-intensive characterization, because rates can be measured in parallel in a short amount of time and do not require large sample quantities (5–10 mg). This advantage could accelerate the iterative process of materials synthesis and pair well with recently developed high-throughput synthesis approaches.[77]

In addition, the prospects for generalizing these methods to metals other than Fe are important as new catalytic applications arise. Mössbauer spectroscopy shows limited generality due to the nature of the Mössbauer effect, whereas the probe molecule and kinetic methods show promise (Table 2). It is worth noting, however, that the specificity of Mössbauer spectroscopy can be an advantage when Fe is present in bimetallic or multimetallic catalysts.[78] Some limitations have been encountered with CO pulse chemisorption. For example, NiN_x centers are not titrated,[58] presumably because they do not adsorb CO strongly enough. This requirement may be somewhat limiting and could also apply to the NO-stripping technique if some MN_x sites do not adsorb NO with sufficient strength. This hypothesis is consistent with recent data from Kucernak and coworkers that show a lack of a clear NO stripping peak on materials containing Zn, Ni, Sn, Sb, Bi, and Mn.[55] Active-site saturation requirements do not limit HQ oxidation, but generality may be limited by different considerations. Each new metal would require the value of TOF_{MNx} to be determined again, which in turn requires sufficiently well-defined materials to establish reliable benchmarks. The extension of metalation strategies to other metals may provide this opportunity. It may also be anticipated that some metals possess a lower intrinsic reactivity that cannot be accurately distinguished from the background reactivity of the metal-free analog; this case is already apparent for the ZnN_x centers likely present in the Fe-free analogs of ZIF-8-derived catalysts studied in this work.

Conclusions

The aerobic oxidation of a sulfonated hydroquinone molecule serves as a catalytic probe reaction for the kinetic quantification of mononuclear FeN_x active centers in Fe-N-C catalysts. The intrinsic turnover frequency of hydroquinone oxidation is assessed using Fe-N-C catalysts that contain solvent-accessible FeN_x centers synthesized by metalation strategies and characterized by low-temperature Mössbauer spectroscopy. The hydroquinone oxidation turnover frequency enables the calculation of the FeN_x active-site density of a suite of Fe-N-C catalysts with varying synthetic provenance and Fe speciation. The collection of fourteen Fe-N-C materials compared in this study encompasses a broader – and thus more representative – sampling of the diversity of Fe-N-C catalysts than previous active-site benchmarking efforts[19] and, thereby, reveals deeper insights into the materials characteristics and fundamental challenges that cause active-site quantification approaches to deviate from one another. These broad comparisons of kinetic, probe-molecular, and spectroscopic approaches to quantify FeN_x centers show that the kinetic method correlates well with CO pulse chemisorption and Mössbauer spectroscopy but does not correlate well with electrochemical NO stripping. Yet, no single quantification strategy is yet suitable to be considered accurate for every Fe-N-C catalyst, highlighting the importance of cross-validation with more than one technique. The 1:1 correlations between three different active-site quantification approaches (HQ, CO, Mössbauer) on more than ten different Fe-N-C materials are unprecedented in the Fe-N-C literature. These correlations provide the basis for the expanded use of active-site quantification in any study that measures the rate of a catalytic reaction on Fe-N-C catalysts, so that reaction rates can be properly compared on a per-site basis.

The kinetic approach to quantify FeN_x centers developed here not only complements existing methods but also offers attractive unique features. The absence of a pretreatment that may alter the state of the catalyst expands the range of catalysts whose site densities can be quantified accurately, such as catalysts synthesized using mild temperatures or those that have undergone extensive aging in a device or other treatments that cause deactivation.[10,53,79] The relative ease of applying the kinetic quantification method should also facilitate its use for rapid screening in conjunction with materials synthesis efforts and drive the broader adoption of active-site benchmarking in areas where it is seldom employed.[7]

Methods

Materials Synthesis

The 2,3,5,6-tetrakis(propylsulfanyl-3'-sulfonate)-1,4-hydroquinone tetrasodium salt (HQ) used in this study was prepared according to a previously reported protocol.[46,47] The synthetic protocol is straightforward, but samples of this material can also be made available to others. For groups interested in obtaining a sample, contact the corresponding author (S. S. Stahl).

Fe-N-C materials reported in this work are generally named "*x*Fe-N-C[descriptor]", where the leading *x* denotes the bulk Fe content quantified by ICP-OES[56] as described in section 1 of the Supporting Information, and [descriptor] provides information about the synthetic route or institution of origin. Fe-N-C materials with low Fe loadings and the majority of Fe in atomically dispersed FeN_x configurations were synthesized by a solution-phase metalation of ZIF-8-derived N-C following our previous report.[13] These materials are labeled as xFe-N-$C^{\text{m-ht}}$, where "m-ht" refers to a metalation followed by a heat treatment. Fe-N-C materials with higher Fe loadings including agglomerated Fe species were synthesized by the same approach, but under an atmosphere containing air, and are labeled xFe-N-$C^{\text{ma-ht}}$ ("ma" = metalation with air). An Fe-N-C material was synthesized by the solution-phase metalation of ZIF-8-derived N-C after a gas-phase HCl treatment, denoted as 0.3Fe-N-$C^{\text{HCl-m-ht}}$ ("HCl-m" = HCl treatment followed by metalation), following our previous report.[13] All materials described above were loaded into a quartz boat and treated within a horizontal tube furnace in flowing N_2 at 873 K (ramp rate = 10 K min^{-1}) for 2 h, then cooled by convection to ambient temperature; this heat treatment is denoted as "$^{\text{ht}}$" in sample names. Further details can be found in the Supporting Information, section 2.2.

The 1.5Fe-Phen-C material was synthesized through the pyrolysis of a carbon-supported Fe complex ligated by 1,10-phenanothroline based on methods reported in the literature [80] and described as "1.5Fe-Phen-C" in our previous publication.[13] The 1.2Fe-PANI-C material was synthesized through pyrolysis of a mixture of carbon, polyaniline, and Fe based on methods reported in the literature[81,82] and described as "1.2Fe-PANI-C" in our previous publications.[48,13]

The 4.7Fe-N-C-ST catalyst was synthesized by a $FeCl_3$/LiCl eutectic salt melt metalation strategy reported previously.[57] Briefly, a Zn-N-C material was prepared by the pyrolysis of 1,2-dicyanobenzene within a $ZnCl_2$/LiCl mixture (60 mol% LiCl) in an Ar atmosphere at 1073 K for 1 h, followed by washing with 0.1 M HCl. Then the Zn-N-C was (trans)metalated at 443 K in a eutectic $FeCl_3$/LiCl salt melt followed by the same acid washing, and a flash pyrolysis at 1273 K for 0.33 h under Ar. The 0.5Fe-N-C UCI catalyst was synthesized by the sacrificial support method, where an iron-nicarbazin mixture is melted into the nanoporous sacrificial silica template via pyrolysis, with subsequent acid etching to remove the silica template and metallic nanoparticles. The process is reported in detail in the literature.[59,60] The synthesis of the 5.7Fe-N-C-TUB catalyst involved aniline polymerization, followed by pyrolysis of a mixture of activated carbon support, Fe precursor, and polyaniline based on methods reported in the literature.[58] The 0.9Fe-N-C-UB material was prepared through the pyrolysis of an Fe_2O_3@ZIF-8 composite under 10% H_2/Ar as reported in the literature. The Fe_2O_3@ZIF-8 composite was prepared according to previous work.[83] For comparison, a 0.8Fe-N-C-UB material was synthesized with an identical Fe_2O_3@ZIF-8 precursor and heat treatment, except that the pyrolysis gas was Ar. The 0.8Fe-N-C-CNRS catalyst was prepared by the pyrolysis of ZIF-8 mixed with $Fe(OAc)_2$ and 1,10-phenanthroline in Ar at 1323 K, as reported previously.[8] A commercially available Fe-N-C catalyst was sourced from Pajarito Powder, LLC[61] (product number PMF-011904), and is referred to as "0.5Fe-N-C-PAJ."

Materials Characterization

^{57}Fe Mössbauer Spectroscopy.—Spectra were collected on a 1024 channel See Co model W304 resonant gamma-ray spectrometer using ^{57}Co on Rh foil as a gamma-ray source. Isomer shifts were referenced to α-Fe foil at room temperature. Fe-N-C samples were loaded into the sample chamber and spectra were collected under vacuum with a source velocity range of ±10 mm s^{-1}. Fe-N-C samples were cooled to 4.2–10 K using a Janis model SHI-850 cryostat controlled by a Lakeshore model 336 temperature controller. Spectra were fit with the VindaD Excel add-in.[84] Fitting details and spectra can be found in section 3.1 of the Supporting Information. All reported Mössbauer spectra were collected at the University of Wisconsin with the exception of 4.7Fe-N-C-ST (at TUM).

CO Pulse Chemisorption.—The density of FeN_x centers in Fe-N-C catalysts was estimated by the adsorption of CO at 195 K following previously reported methods.[33,36] Fe-N-C materials were supported between two quartz wool plugs within a U-shaped quartz tube loaded onto a Micromeritics Autochem II 2920 Chemisorption instrument equipped with a residual gas analyzer (MKS Cirrus) for effluent analysis and a Micromeritics CryoCooler accessory for sub-ambient temperature control. The temperature of the bed was controlled with a quartz-sheathed thermocouple in contact with the upper quartz wool plug. Fe-N-C materials were treated in flowing He (UHP, Airgas, 50 cm^3 min^{-1}) to 873 K (10 K min^{-1}) for 0.25 h, allowed to cool to ambient temperature, then further cooled to 195 K (5 K min^{-1}) using the CryoCooler accessory. During this cooling step, a separate gas stream of 5% CO/He was introduced to a sample loop of 500 µL volume held at 383 K and continuously flowed at a rate of 50 cm^3 min^{-1}. The system was allowed to dwell after cooling to 195 K for 0.25 h to allow for equilibration of the sample temperature and RGA signal, then pulsing of the CO from the sample loop was started. A pulse was executed as follows: the CO/He flow in the loop was stopped for 30 s to ensure pressure equilibration in the loop (P = 1 bar), then the 6-port valve was switched to direct the He carrier gas stream through the CO-containing sample loop; He carrier gas was allowed to flow through the sample loop for 300 s, then the 6-port valve was switched back to allow the sample loop to fill with CO/He for 270 s. This pulsing procedure was repeated ten times to ensure that a minimum of three CO peaks (m/z = 28) at the end of the experiment were of equivalent area, indicating saturation of FeN_x sites with CO. After CO saturation was complete, the sample was allowed to dwell in flowing He at 195 K for 0.25 h, then heated to 873 K (10 K min^{-1}) and held for 0.25 h to desorb CO and with the intent to return the surface to the same state as before CO adsorption. The molar quantity of CO per pulse (N_{pulse}) was calculated assuming the ideal gas law in the loop (P = 1 bar, T = 383 K, V = 500 μL, CO mole fraction = 0.05), and the RGA peak area (m/z = 28) corresponding to this quantity (A_{tot}) was calculated as the average peak area of the final ≥3 pulses of approximately equivalent area. The amount of CO adsorbed in each pulse was then calculated as $N_{ads} = N_{pulse}(1 - A_{pulse}/A_{tot})$, and the cumulative amount of CO adsorbed over all ten pulses to reach saturation was assumed to reflect the density of FeN_x sites in the material. A summary of CO-titrated FeN_x densities and all pulsing profiles can be found in section 3.2 of the Supporting Information. All reported CO pulse chemisorption data were collected at the University of Wisconsin with the exception of 4.7Fe-N-C-ST (at Technical University Berlin as previously reported[19,36]).

Reductive Stripping of NO derived from NO_2^-.—The density of FeN_x centers was estimated from the reductive stripping of NO derived from NO_2^- on a subset of Fe-N-C catalysts using previously reported methods[34] including a modified cleaning protocol reported later.[39] Fe-N-C films were deposited on a glassy carbon rotating disk electrode (RDE) with a diameter of 5 mm housed within a cylindrical PTFE shroud (Pine Research Instrumentation, E6R1 ChangeDisk), which served as the working electrode (WE). Catalyst inks composed of 5 mg of Fe-N-C with 54 μL of Nafion solution (5 wt% in mixture of lower aliphatic alcohols and water, Sigma-Aldrich), 530 μL of isopropanol (≥99.5%, Sigma-Aldrich), and 530 μL of H_2O (18.2 MΩ cm) were sonicated in an ice-water bath for 1 h. The electrode was polished with a 0.05 μm alumina suspension (BASi) on a polishing pad, then sonicated in methanol (Avantor, anhydrous) for 0.25 h. The electrode was mounted on the rotator in an inverted configuration and rotated at ~100 rpm. While rotating the electrode, an aliquot of the catalyst ink was deposited on the electrode to achieve a loading of 0.2 mg cm^{-2} of catalyst on the electrode, as quantified by the volume of ink dispensed from a volumetric displacement pipet (Eppendorf, 20 μL). The film was allowed to dry at ambient temperature for >0.33 h. The WE was immersed in 15–20 mL of a 0.5 M acetate buffer (HOAc/NaOAc) at a pH of 5.2 within a 25 mL four-neck round-bottomed flask equipped with a Ag/AgCl reference electrode, graphite rod counter electrode, and PTFE gas-purge tube. The electrodes were connected to a potentiostat (BioLogic BP-300), and potentials were converted to the reversible hydrogen electrode (RHE) scale using the relationship $E_{RHE} = E_{Ag/AgCl} + 0.059pH + 0.1976\,V$.

The catalyst film was pretreated using sequential cyclic voltammetry (CV) scans without electrode rotation while the electrolyte was saturated with either O_2 (>99.2%, Airgas) or

Ar (99.998%, Airgas). Pretreatment CVs were performed between 1.05 and −0.4 V_{RHE} as follows: (a) three repetitions under O_2 at 5 mV s^{-1}, (b) 20 repetitions under Ar at 100 mV s^{-1}, (c) 10 repetitions under Ar at 10 mV s^{-1}, then (a)–(c) again, then one final treatment described in (a). After this, (d) a linear sweep voltammogram (LSV) was recorded under O_2 from 1.0 to 0.3 V_{RHE} at 5 mV s^{-1} while rotating at 1600 rpm and is denoted the "unpoisoned" LSV. Then, under Ar, without rotation, a "pre-baseline" CV (e) was performed from 1.0 to 0.3 V_{RHE} at 10 mV s^{-1}, with the intent to equilibrate the system, followed by a "baseline" CV (f) from 0.4 to −0.3 V_{RHE} at 10 mV s^{-1}. The "baseline" CV (f) was preceded by a 30 s hold at 0.4 V_{RHE} to further ensure equilibration and a reproducible current density. The "pre-baseline" CV (e) was used to correct LSV data, and the "baseline" CV (f) was used as the reference for the NO stripping CV (g, below).

Next, at open-circuit potential, the WE was rotated at 300 rpm and immersed in ~15 mL of an aqueous 0.125 $NaNO_2$ solution (≥97%, Sigma-Aldrich) for 300 s. The WE was then immersed in ~15 mL of H_2O (18.2 MΩ cm) for 60 s, then in ~15 mL of the electrolyte solution (pH 5.2 acetate buffer) for 600 s, then in a fresh ~15 mL of H_2O for 60 s. The WE was then returned to the cell under O_2-saturated electrolyte and an LSV was recorded under the same conditions described in (d), referred to as the "poisoned" LSV. Then, in Ar-saturated electrolyte and without rotation, the "pre-baseline" CV (e) was recorded, followed by an equilibration for 30 s holding the potential at 0.4 V_{RHE}, and then a CV (g) from 0.4 to −0.3 V_{RHE} at 10 mV s^{-1}, referred to as the "stripping" CV. Another LSV in O_2-saturated electrolyte was recorded under the same conditions described in (d), referred to as the "recovered" LSV. These LSVs are used to confirm the success of NO poisoning. After measurement of the "recovered" LSV, the same poisoning steps described above were performed, and following poisoning the "pre-baseline" (e) and "stripping" (g) CVs were recorded. This stripping CV was compared with the "baseline" CV (f) to quantify the amount of NO stripped. This second poisoning and stripping protocol was adopted to ensure that the stripping curve was not perturbed by exposure to O_2 during the "poisoned" ORR LSV, as recommended in a recent report.[39] The "pre-baseline" (e) and "baseline" (f) steps were repeated after this final stripping, which was recently reported by the same group to be suitable for baseline correction.[55] The FeN_x site density (N_{FeNx}, mol g^{-1}) was calculated according to the following equation:

$$N_{FeN_x} = \frac{Q_{strip}}{n_{strip}F} \tag{5}$$

where Q_{strip} (C g^{-1}) is the charge associated with the reductive stripping of NO, F is Faraday's constant (C mol^{-1}), and n_{strip} is the number of electrons associated with the reduction of a NO–FeN_x species. The value of n_{strip} was assumed to be 3 according to reports that the product of NO reduction on Fe-N-C catalysts is NH_2OH,[41,35] that is: $NO - FeN_x + 3H^+ + 3e^- \rightarrow FeN_x + NH_2OH$. A step-by-step form of this procedure can be found in section 3.3.1 of the Supporting Information. A summary of NO-titrated FeN_x densities using both 3-electron and 5-electron stripping assumptions with all possible combinations of stripping and baseline voltammograms, and all relevant LSV and CV data can be found in section 3.3.3 of the Supporting Information. All reported NO stripping data were collected at the University of Wisconsin.

Hydroquinone Oxidation Kinetic Measurements

2,3,5,6-Tetrakis(propylsulfanyl-3'-sulfonate)-1,4-hydroquinone tetrasodium salt (HQ) was prepared according to our previous publication.[46,47] In a typical experiment, M–N–C samples (5–20 mg) were combined with 0.5 M H_2SO_4 (10–20 mL, prepared using 18.2 MΩ cm H_2O) and mixed at 2.3×10^4 rpm for >180 s using a stainless-steel dispersing tool (IKA S 18 N - 10 G), resulting in aggregates <50 μm. Aliquots (20–750 μL) of this well-mixed dispersion were weighed into separate disposable thick-walled borosilicate glass tubes (10 mL), and additional 0.5 M H_2SO_4 was weighed into each to give a total volume of ~750 μL. The purpose of these preparation steps is to ensure that systematically varying and accurate quantities of catalyst <1 mg are weighed into separate tubes so that the rate can be efficiently quantified in parallel as a function of catalyst loading at constant reaction time. The reactor tubes were loaded into a large-capacity orbital mixer (Glas-Col) equipped with an aluminum heating block that covers the base of the tubes (3 cm), an aluminum cooling block located 7.5 cm from the base of the tubes controlled by a recirculating chiller, and a gas manifold sealed above the cooling block by viton o-rings and rubber septa. The heating block and cooling block were set to 30 °C and 10 °C, respectively, >0.5 h before loading reactor tubes. The system was pressurized with O_2 (99%, Airgas) to 1.1 bar and evacuated then pressurized for 5 cycles to displace air, then sealed at 1.1 bar under O_2. The reaction pressure was set slightly above 1 bar to facilitate initial pressure testing of the system prior to reaction. The assembly was mixed at a rotation rate of 1200 rpm for >300 s before starting the reaction. A 250 μL aliquot of a 0.2 M solution of HQ in 0.5 M H_2SO_4 was injected via syringe (Hamilton) into each reactor tube through the rubber septa to initiate the reaction, and the time of injection was noted as the initial time (t_0) for each reactor tube. After 0.33 h, the pressure was lowered to 1 bar, and the solutions were withdrawn through the septa into disposable syringes and passed through 0.2 μm PTFE filters to complete the reaction. The filtration time of each reaction solution was noted as the final time (t_f) to calculate the overall reaction time ($t_f - t_0$). An aliquot of each product solution (~310 mg) was combined with ~330 mg of a 10–60 mM stock solution of pivalic acid (99%) in D_2O (99.9 % atom D) as an internal standard and analyzed by ^{1}H NMR spectroscopy to quantify quinone products and unreacted hydroquinone (see Figure S41 in the Supporting Information for a representative spectrum). A catalyst-free blank was included in every run and used as the initial time reference. Mass balances were generally calculated to be 100 ± 5%. The error associated with these rate measurements was estimated by independent replicates in our previous work[13] to be ± 20%. A summary of FeN_x densities estimated by HQ oxidation and all initial rate data can be found in section 4.3 of the Supporting Information. All reported HQ oxidation data were collected at the University of Wisconsin.

Note: Samples of the HQ may be obtained by contacting the corresponding author (S. S. Stahl). Further discussion of the procedure for calculating initial rates of HQ oxidation and considerations of transport limitations, which are essential for accurate site quantitation, are included in sections 4.1 and 4.2 of the Supporting Information.

Supplementary Material

Refer to Web version on PubMed Central for supplementary material.

ACKNOWLEDGMENTS

The authors thank Cathy Clewett for assistance with Mössbauer spectroscopy, Fatemeh Khamespanah for assistance with materials synthesis, and Edgard Lebrón-Rodríguez and Ive Hermans for access to instrumentation for CO pulse chemisorption measurements. This research was supported by the U.S. Department of Energy, Office of Science, Basic Energy Sciences, under award no. DE-FG02-05ER15690, and by a Ruth L. Kirschstein NRSA fellowship from the NIH (F32GM137472, to J.S.B.). Spectroscopic instrumentation was partially supported by the NIH (1S10 OD020022-1) and the NSF (CHE-1048642). The Mössbauer MS4 spectrometer was supported by the Department of Chemistry, University of Wisconsin–Madison. ICP-OES instrumentation at the Water Sciences Engineering Laboratory was supported by the University of Wisconsin. The UCI components of this work were funded by US Department of Energy, Office of Energy Efficiency and Renewable Energy (EERE), through the Advanced Manufacturing Office program to Sandia National Laboratories (AOP 34920). This project received financial support from the German Federal Ministry of Education and Research (BMBF) through grant 03XP0251 (“KorrZellKat”). Funding by the German Research Foundation (DFG) within the framework of the priority program SPP 2240 (research project FE 1590/1-1) is gratefully acknowledged by BAM. F. J. acknowledges financial support from the French National Research Agency through the ANIMA project (grant number ANR-19-CE05-0039). G. W. acknowledges partial support from the National Science Foundation (CBET - 1804326 and 2223467).

References

1. Gewirth AA; Varnell JA; DiAscro AM Nonprecious Metal Catalysts for Oxygen Reduction in Heterogeneous Aqueous Systems. Chem. Rev 2018, 118, 2313–2339. [PubMed: 29384375]
2. He Y; Liu S; Priest C; Shi Q; Wu G Atomically Dispersed Metal–Nitrogen–Carbon Catalysts for Fuel Cells: Advances in Catalyst Design, Electrode Performance, and Durability Improvement. Chem. Soc. Rev 2020, 49, 3484–3524. [PubMed: 32342064]
3. Martinez U; Komini Babu S; Holby EF; Chung HT; Yin X; Zelenay P Progress in the Development of Fe-Based PGM-Free Electrocatalysts for the Oxygen Reduction Reaction. Adv. Mater 2019, 31, 1806545.
4. Asset T; Atanassov P Iron-Nitrogen-Carbon Catalysts for Proton Exchange Membrane Fuel Cells. Joule 2020, 4, 33–44.
5. He L; Weniger F; Neumann H; Beller M Synthesis, Characterization, and Application of Metal Nanoparticles Supported on Nitrogen-Doped Carbon: Catalysis beyond Electrochemistry. Angew. Chem. Int. Ed 2016, 55, 12582–12594.
6. Singh B; Gawande MB; Kute AD; Varma RS; Fornasiero P; McNeice P; Jagadeesh RV; Beller M; Zbořil R Single-Atom (Iron-Based) Catalysts: Synthesis and Applications. Chem. Rev 2021, 121, 13620–13697. [PubMed: 34644065]
7. Bates JS; Johnson MR; Khamespanah F; Root TW; Stahl SS Heterogeneous M-N-C Catalysts for Aerobic Oxidation Reactions: Lessons from Oxygen Reduction Electrocatalysts. Chem. Rev 2023, 123, 6233–6256. [PubMed: 36198176]
8. Zitolo A; Goellner V; Armel V; Sougrati M-T; Mineva T; Stievano L; Fonda E; Jaouen F Identification of Catalytic Sites for Oxygen Reduction in Iron- and Nitrogen-Doped Graphene Materials. Nat. Mater 2015, 14, 937–942. [PubMed: 26259106]
9. Chung HT; Cullen DA; Higgins D; Sneed BT; Holby EF; More KL; Zelenay P Direct Atomic-Level Insight into the Active Sites of a High-Performance PGM-Free ORR Catalyst. Science 2017, 357, 479–484. [PubMed: 28774924]
10. Li J; Sougrati MT; Zitolo A; Ablett JM; Oğuz IC; Mineva T; Matanovic I; Atanassov P; Huang Y; Zenyuk I; Di Cicco A; Kumar K; Dubau L; Maillard F; Dražić G; Jaouen F Identification of Durable and Non-Durable FeN_x Sites in Fe–N–C Materials for Proton Exchange Membrane Fuel Cells. Nat. Catal 2021, 4, 10–19.
11. Xie J; Yin K; Serov A; Artyushkova K; Pham HN; Sang X; Unocic RR; Atanassov P; Datye AK; Davis RJ Selective Aerobic Oxidation of Alcohols over Atomically-Dispersed Non-Precious Metal Catalysts. ChemSusChem 2017, 10, 359–362. [PubMed: 27863066]
12. Xie J; Kammert JD; Kaylor N; Zheng JW; Choi E; Pham HN; Sang X; Stavitski E; Attenkofer K; Unocic RR; Datye AK; Davis RJ Atomically Dispersed Co and Cu on N-Doped Carbon for Reactions Involving C–H Activation. ACS Catal. 2018, 8, 3875–3884.

13. Bates JS; Khamespanah F; Cullen DA; Al-Omari AA; Hopkins MN; Martinez JJ; Root TW; Stahl SS Molecular Catalyst Synthesis Strategies to Prepare Atomically Dispersed Fe-N-C Heterogeneous Catalysts. J. Am. Chem. Soc 2022, 144, 18797–18802. [PubMed: 36215721]
14. Boudart M Turnover Rates in Heterogeneous Catalysis. Chem. Rev 1995, 95, 661–666.
15. Davis R Turnover Rates on Complex Heterogeneous Catalysts. AIChE J. 2018, 64, 3778–3785.
16. Esposito D Induce to Reproduce. Nat. Catal 2022, 5, 658–661.
17. Addressing Rigor and Reproducibility in Thermal, Heterogeneous Catalysis (NSF Workshop Report). June 12, 2023. DOI: 10.5281/zenodo.8029159
18. Li J; Jaouen F Structure and Activity of Metal-Centered Coordination Sites in Pyrolyzed Metal–Nitrogen–Carbon Catalysts for the Electrochemical Reduction of O_2. Curr. Opin. Electrochem 2018, 9, 198–206.
19. Primbs M; Sun Y; Roy A; Malko D; Mehmood A; Sougrati M-T; Blanchard P-Y; Granozzi G; Kosmala T; Daniel G; Atanassov P; Sharman J; Durante C; Kucernak A; Jones D; Jaouen F; Strasser P Establishing Reactivity Descriptors for Platinum Group Metal (PGM)-Free Fe–N–C Catalysts for PEM Fuel Cells. Energy Environ. Sci 2020, 13, 2480–2500.
20. Snitkoff-Sol RZ; Elbaz L Assessing and Measuring the Active Site Density of PGM-Free ORR Catalysts. J. Solid State Electrochem 2022, 26, 1839–1850.
21. Specchia S; Atanassov P; Zagal JH Mapping Transition Metal–Nitrogen–Carbon Catalyst Performance on the Critical Descriptor Diagram. Curr. Opin. Electrochem 2021, 27, 100687.
22. Kozhushner A; Zion N; Elbaz L Methods for Assessment and Measurement of the Active Site Density in Platinum Group Metal–Free Oxygen Reduction Reaction Catalysts. Curr. Opin. Electrochem 2021, 25, 100620.
23. Luo F; Wagner S; Ju W; Primbs M; Li S; Wang H; Kramm UI; Strasser P Kinetic Diagnostics and Synthetic Design of Platinum Group Metal-Free Electrocatalysts for the Oxygen Reduction Reaction Using Reactivity Maps and Site Utilization Descriptors. J. Am. Chem. Soc 2022, 144, 13487–13498. [PubMed: 35862859]
24. van Veen JAR; van Baar JF; Kroese KJ Effect of Heat Treatment on the Performance of Carbon-Supported Transition-Metal Chelates in the Electrochemical Reduction of Oxygen. J. Chem. Soc., Faraday Trans. 1 1981, 77, 2827–2843.
25. Schulenburg H; Stankov S; Schünemann V; Radnik J; Dorbandt I; Fiechter S; Bogdanoff P; Tributsch H Catalysts for the Oxygen Reduction from Heat-Treated Iron(III) Tetramethoxyphenylporphyrin Chloride: Structure and Stability of Active Sites. J. Phys. Chem. B 2003, 107, 9034–9041.
26. Wagner S; Auerbach H; Tait CE; Martinaiou I; Kumar SCN; Kübel C; Sergeev I; Wille H-C; Behrends J; Wolny JA; Schünemann V; Kramm UI Elucidating the Structural Composition of an Fe–N–C Catalyst by Nuclear- and Electron-Resonance Techniques. Angew. Chem. Int. Ed 2019, 58, 10486–10492.
27. Mineva T; Matanovic I; Atanassov P; Sougrati M-T; Stievano L; Clémancey M; Kochem A; Latour J-M; Jaouen F Understanding Active Sites in Pyrolyzed Fe–N–C Catalysts for Fuel Cell Cathodes by Bridging Density Functional Theory Calculations and ^{57}Fe Mössbauer Spectroscopy. ACS Catal. 2019, 9, 9359–9371.
28. Sougrati MT; Goellner V; Schuppert AK; Stievano L; Jaouen F Probing Active Sites in Iron-Based Catalysts for Oxygen Electro-Reduction: A Temperature-Dependent ^{57}Fe Mössbauer Spectroscopy Study. Catal. Today 2016, 262, 110–120.
29. Kramm UI; Ni L; Wagner S ^{57}Fe Mössbauer Spectroscopy Characterization of Electrocatalysts. Adv. Mater 2019, 31, 1805623.
30. Kramm UI; Lefèvre M; Larouche N; Schmeisser D; Dodelet J-P Correlations between Mass Activity and Physicochemical Properties of Fe/N/C Catalysts for the ORR in PEM Fuel Cell via ^{57}Fe Mössbauer Spectroscopy and Other Techniques. J. Am. Chem. Soc 2014, 136, 978–985. [PubMed: 24345296]
31. Kneebone JL; Daifuku SL; Kehl JA; Wu G; Chung HT; Hu MY; Alp EE; More KL; Zelenay P; Holby EF; Neidig ML A Combined Probe-Molecule, Mössbauer, Nuclear Resonance Vibrational Spectroscopy, and Density Functional Theory Approach for Evaluation of Potential Iron Active Sites in an Oxygen Reduction Reaction Catalyst. J. Phys. Chem. C 2017, 121, 16283–16290.

32. Ni L; Gallenkamp C; Wagner S; Bill E; Krewald V; Kramm UI Identification of the Catalytically Dominant Iron Environment in Iron- and Nitrogen-Doped Carbon Catalysts for the Oxygen Reduction Reaction. J. Am. Chem. Soc 2022, 144, 16827–16840. [PubMed: 36036727]
33. Sahraie NR; Kramm UI; Steinberg J; Zhang Y; Thomas A; Reier T; Paraknowitsch J-P; Strasser P Quantifying the Density and Utilization of Active Sites in Non-Precious Metal Oxygen Electroreduction Catalysts. Nat. Commun 2015, 6, 8618. [PubMed: 26486465]
34. Malko D; Kucernak A; Lopes T In Situ Electrochemical Quantification of Active Sites in Fe–N/C Non-Precious Metal Catalysts. Nat. Commun 2016, 7, 13285. [PubMed: 27796287]
35. Bae G; Kim H; Choi H; Jeong P; Kim DH; Kwon HC; Lee K-S; Choi M; Oh H-S; Jaouen F; Choi CH Quantification of Active Site Density and Turnover Frequency: From Single-Atom Metal to Nanoparticle Electrocatalysts. JACS Au 2021, 1, 586–597. [PubMed: 34467322]
36. Luo F; Choi CH; Primbs MJM; Ju W; Li S; Leonard ND; Thomas A; Jaouen F; Strasser P Accurate Evaluation of Active-Site Density (SD) and Turnover Frequency (TOF) of PGM-Free Metal–Nitrogen-Doped Carbon (MNC) Electrocatalysts Using CO Cryo Adsorption. ACS Catal. 2019, 9, 4841–4852.
37. Leonard ND; Wagner S; Luo F; Steinberg J; Ju W; Weidler N; Wang H; Kramm UI; Strasser P Deconvolution of Utilization, Site Density, and Turnover Frequency of Fe–Nitrogen–Carbon Oxygen Reduction Reaction Catalysts Prepared with Secondary N-Precursors. ACS Catal. 2018, 8, 1640–1647.
38. Malko D; Kucernak A; Lopes T Performance of Fe–N/C Oxygen Reduction Electrocatalysts toward NO2–, NO, and NH_2OH Electroreduction: From Fundamental Insights into the Active Center to a New Method for Environmental Nitrite Destruction. J. Am. Chem. Soc 2016, 138, 16056–16068. [PubMed: 27960317]
39. Mehmood A; Gong M; Jaouen F; Roy A; Zitolo A; Khan A; Sougrati M-T; Primbs M; Bonastre AM; Fongalland D; Drazic G; Strasser P; Kucernak A High Loading of Single Atomic Iron Sites in Fe–NC Oxygen Reduction Catalysts for Proton Exchange Membrane Fuel Cells. Nat. Catal 2022, 5, 311–323.
40. Li J; Jiao L; Wegener E; Richard LL; Liu E; Zitolo A; Sougrati MT; Mukerjee S; Zhao Z; Huang Y; Yang F; Zhong S; Xu H; Kropf AJ; Jaouen F; Myers DJ; Jia Q Evolution Pathway from Iron Compounds to Fe_1(II)–N_4 Sites through Gas-Phase Iron during Pyrolysis. J. Am. Chem. Soc 2020, 142, 1417–1423. [PubMed: 31880925]
41. Kim DH; Ringe S; Kim H; Kim S; Kim B; Bae G; Oh H-S; Jaouen F; Kim W; Kim H; Choi CH Selective Electrochemical Reduction of Nitric Oxide to Hydroxylamine by Atomically Dispersed Iron Catalyst. Nat. Commun 2021, 12, 1856. [PubMed: 33767159]
42. Menga D; Guilherme Buzanich A; Wagner F; Fellinger T-P Evaluation of the Specific Activity of M−N−Cs and the Intrinsic Activity of Tetrapyrrolic FeN_4 Sites for the Oxygen Reduction Reaction. Angew. Chem. Int. Ed 2022, 61, e202207089.
43. Snitkoff-Sol RZ; Friedman A; Honig HC; Yurko Y; Kozhushner A; Zachman MJ; Zelenay P; Bond AM; Elbaz L Quantifying the Electrochemical Active Site Density of Precious Metal-Free Catalysts in Situ in Fuel Cells. Nat. Catal 2022, 5, 163–170.
44. Jin Z; Li P; Meng Y; Fang Z; Xiao D; Yu G Understanding the Inter-Site Distance Effect in Single-Atom Catalysts for Oxygen Electroreduction. Nat. Catal 2021, 4, 615–622.
45. Jin Z; Li P; Fang Z; Yu G Emerging Electrochemical Techniques for Probing Site Behavior in Single-Atom Electrocatalysts. Acc. Chem. Res 2022, 55, 759–769. [PubMed: 35148075]
46. Preger Y; Gerken JB; Biswas S; Anson CW; Johnson MR; Root TW; Stahl SS Quinone-Mediated Electrochemical O2 Reduction Accessing High Power Density with an Off-Electrode Co-N/C Catalyst. Joule 2018, 2, 2722–2731.
47. Gerken JB; Stamoulis A; Suh S-E; Fischer ND; Kim YJ; Guzei IA; Stahl SS Efficient Electrochemical Synthesis of Robust, Densely Functionalized Water Soluble Quinones. Chem. Commun 2020, 56, 1199–1202.
48. Bates JS; Biswas S; Suh S-E; Johnson MR; Mondal B; Root TW; Stahl SS Chemical and Electrochemical O_2 Reduction on Earth-Abundant M-N-C Catalysts and Implications for Mediated Electrolysis. J. Am. Chem. Soc 2022, 144, 922–927. [PubMed: 34985869]

49. Mehmood A; Pampel J; Ali G; Ha HY; Ruiz-Zepeda F; Fellinger T-P Facile Metal Coordination of Active Site Imprinted Nitrogen Doped Carbons for the Conservative Preparation of Non-Noble Metal Oxygen Reduction Electrocatalysts. Adv. Energy Mater 2018, 8, 1701771.

50. Menga D; Ruiz-Zepeda F; Moriau L; Šala M; Wagner F; Koyutürk B; Bele M; Petek U; Hodnik N; Gaberšček M; Fellinger T-P Active-Site Imprinting: Preparation of Fe–N–C Catalysts from Zinc Ion–Templated Ionothermal Nitrogen-Doped Carbons. Adv. Energy Mater 2019, 9, 1902412.

51. Tang J; Salunkhe RR; Liu J; Torad NL; Imura M; Furukawa S; Yamauchi Y Thermal Conversion of Core–Shell Metal–Organic Frameworks: A New Method for Selectively Functionalized Nanoporous Hybrid Carbon. J. Am. Chem. Soc 2015, 137, 1572–1580. [PubMed: 25580699]

52. Jiao L; Li J; Richard LL; Sun Q; Stracensky T; Liu E; Sougrati MT; Zhao Z; Yang F; Zhong S; Xu H; Mukerjee S; Huang Y; Cullen DA; Park JH; Ferrandon M; Myers DJ; Jaouen F; Jia Q Chemical Vapour Deposition of Fe–N–C Oxygen Reduction Catalysts with Full Utilization of Dense Fe–N_4 Sites. Nat. Mater 2021, 20, 1385–1391. [PubMed: 34112977]

53. Kumar K; Dubau L; Mermoux M; Li J; Zitolo A; Nelayah J; Jaouen F; Maillard F On the Influence of Oxygen on the Degradation of Fe-N-C Catalysts. Angew. Chem. Int. Ed 2020, 59, 3235–3243.

54. Jiang W-J; Gu L; Li L; Zhang Y; Zhang X; Zhang L-J; Wang J-Q; Hu J-S; Wei Z; Wan L-J Understanding the High Activity of Fe–N–C Electrocatalysts in Oxygen Reduction: Fe/Fe_3C Nanoparticles Boost the Activity of Fe–N_x. J. Am. Chem. Soc 2016, 138, 3570–3578. [PubMed: 26906342]

55. Gong M; Mehmood A; Ali B; Nam K-W; Kucernak A Oxygen Reduction Reaction Activity in Non-Precious Single-Atom (M–N/C) Catalysts—Contribution of Metal and Carbon/Nitrogen Framework-Based Sites. ACS Catal. 2023, 13, 6661–6674. [PubMed: 37229434]

56. We note that the Fe contents of all materials reported in this study were measured by ICP-OES in the same laboratory (at the University of Wisconsin) using identical procedures described in section 1 of the Supporting Information.

57. Menga D; Low JL; Li Y-S; Arčon I; Koyutürk B; Wagner F; Ruiz-Zepeda F; Gaberšček M; Paulus B; Fellinger T-P Resolving the Dilemma of Fe–N–C Catalysts by the Selective Synthesis of Tetrapyrrolic Active Sites via an Imprinting Strategy. J. Am. Chem. Soc 2021, 143, 18010–18019. [PubMed: 34689551]

58. Luo F; Wagner S; Onishi I; Selve S; Li S; Ju W; Wang H; Steinberg J; Thomas A; Kramm UI; Strasser P Surface Site Density and Utilization of Platinum Group Metal (PGM)-Free Fe–NC and FeNi–NC Electrocatalysts for the Oxygen Reduction Reaction. Chem. Sci 2021, 12, 384–396.

59. Huang Y; Chen Y; Xu M; Asset T; Tieu P; Gili A; Kulkarni D; De Andrade V; De Carlo F; Barnard HS; Doran A; Parkinson DY; Pan X; Atanassov P; Zenyuk IV Catalysts by Pyrolysis: Direct Observation of Chemical and Morphological Transformations Leading to Transition Metal-Nitrogen-Carbon Materials. Mater. Today 2021, 47, 53–68.

60. Chen Y; Huang Y; Xu M; Asset T; Yan X; Artyushkova K; Kodali M; Murphy E; Ly A; Pan X; Zenyuk IV; Atanassov P Catalysts by Pyrolysis: Direct Observation of Transformations during Re-Pyrolysis of Transition Metal-Nitrogen-Carbon Materials Leading to State-of-the-Art Platinum Group Metal-Free Electrocatalyst. Mater. Today 2022, 53, 58–70.

61. Pajarito Powder Fuel Cell Catalysts/Products/Precious-Metal-Free™ (PMF) Catalysts. URL https://pajaritopowder.com/products/#PMF (accessed 2023-09-17).

62. Zeng Y; Li C; Li B; Zachman M; Alp E; Karakalos S; Lucero M; Zhang B; Wang M; Feng Z; Wang G; Xie J; Cullen D; Myers D; Dodelet J-P; Wu G Challenging the Activity-Durability Tradeoff of Fe-N-C Fuel Cell Catalysts via Controlling Thermal Activation Atmosphere. ChemRxiv 2022 10.26434/chemrxiv-2022-g4zj8 (accessed 2023-09-17).

63. Kündig W; Bömmel H; Constabaris G; Lindquist RH Some Properties of Supported Small α–Fe_2O_3 Particles Determined with the Mössbauer Effect. Phys. Rev 1966, 142, 327–333.

64. van der Kraan AM Mössbauer Effect Studies of Surface Ions of Ultrafine α-Fe_2O_3 Particles. phys. stat. sol. (a) 1973, 18, 215–226.

65. Niemantsverdriet JW; van der Kraan AM; Delgass WN; Vannice MA Small-Particle Effects in Moessbauer Spectra of a Carbon-Supported Iron Catalyst. J. Phys. Chem 1985, 89, 67–72.

66. Serov A; Artyushkova K; Niangar E; Wang C; Dale N; Jaouen F; Sougrati M-T; Jia Q; Mukerjee S; Atanassov P Nano-Structured Non-Platinum Catalysts for Automotive Fuel Cell Application. Nano Energy 2015, 16, 293–300.
67. Jia Q; Ramaswamy N; Tylus U; Strickland K; Li J; Serov A; Artyushkova K; Atanassov P; Anibal J; Gumeci C; Barton SC; Sougrati M-T; Jaouen F; Halevi B; Mukerjee S Spectroscopic Insights into the Nature of Active Sites in Iron–Nitrogen–Carbon Electrocatalysts for Oxygen Reduction in Acid. Nano Energy 2016, 29, 65–82.
68. Boldrin P; Malko D; Mehmood A; Kramm UI; Wagner S; Paul S; Weidler N; Kucernak A Deactivation, Reactivation and Super-Activation of Fe-N/C Oxygen Reduction Electrocatalysts: Gas Sorption, Physical and Electrochemical Investigation Using NO and O_2. Appl. Catal., B 2021, 292, 120169.
69. Wang Q; Yang Y; Sun F; Chen G; Wang J; Peng L; Chen W-T; Shang L; Zhao J; Sun-Waterhouse D; Zhang T; Waterhouse GIN Molten NaCl-Assisted Synthesis of Porous Fe-N-C Electrocatalysts with a High Density of Catalytically Accessible FeN_4 Active Sites and Outstanding Oxygen Reduction Reaction Performance. Adv. Energy Mater 2021, 11, 2100219.
70. Zou J; Chen C; Chen Y; Zhu Y; Cheng Q; Zou L; Zou Z; Yang H Facile Steam-Etching Approach to Increase the Active Site Density of an Ordered Porous Fe–N–C Catalyst to Boost Oxygen Reduction Reaction. ACS Catal. 2022, 12, 4517–4525.
71. Chen G; An Y; Liu S; Sun F; Qi H; Wu H; He Y; Liu P; Shi R; Zhang J; Kuc A; Kaiser U; Zhang T; Heine T; Wu G; Feng X Highly Accessible and Dense Surface Single Metal FeN4 Active Sites for Promoting the Oxygen Reduction Reaction. Energy Environ. Sci 2022, 15, 2619–2628.
72. The spread in the isomer shift and quadrupole splitting values exhibited by D1 (and D2) among different catalysts (see section 3.1 in the Supporting Information) can reflect a diversity of local coordination environments for FeN_x sites. This site-diversity could be an additional contributor to the scatter in correlations. This interpretation is supported by an article published during the revision of our manuscript, which reports a much narrower set of Mössbauer parameters for a solid catalyst with better-defined Fe-N-C sites with a tetrahedral $Fe^{II}N_2Cl_2$ coordination: Genoux A; Pauly M; Rooney CL; Choi C; Shang B; McGuigan S; Fataftah MS; Kayser Y; Suhr SCB; DeBeer S; Wang H; Maggard PA; Holland PL Well-Defined Iron Sites in Crystalline Carbon Nitride. J. Am. Chem. Soc 2023. 10.1021/jacs.3c05417.
73. Feng K; Zhang H; Gao J; Xu J; Dong Y; Kang Z; Zhong J Single Atoms or Not? The Limitation of EXAFS. Appl. Phys. Lett 2020, 116, 191903.
74. Finzel J; Sanroman Gutierrez KM; Hoffman AS; Resasco J; Christopher P; Bare SR Limits of Detection for EXAFS Characterization of Heterogeneous Single-Atom Catalysts. ACS Catal. 2023, 13, 6462–6473.
75. Luo F; Roy A; Silvioli L; Cullen DA; Zitolo A; Sougrati MT; Oguz IC; Mineva T; Teschner D; Wagner S; Wen J; Dionigi F; Kramm UI; Rossmeisl J; Jaouen F; Strasser PP -Block Single-Metal-Site Tin/Nitrogen-Doped Carbon Fuel Cell Cathode Catalyst for Oxygen Reduction Reaction. Nat. Mater 2020, 19, 1215–1223. [PubMed: 32661387]
76. Martinez U; Holby EF; Babu SK; Artyushkova K; Lin L; Choudhury S; Purdy GM; Zelenay P Experimental and Theoretical Trends of PGM-Free Electrocatalysts for the Oxygen Reduction Reaction with Different Transition Metals. J. Electrochem. Soc 2019, 166, F3136.
77. Ferrandon MS; Park JH; Wang X; Coleman E; Jeremy Kropf A; Myers DJ Enhancing the Activity of Fe-N-C Oxygen Reduction Reaction Electrocatalysts by High-Throughput Exploration of Synthesis Parameters. Electrochim. Acta 2023, 441, 141850.
78. Luo F; Roy A; Sougrati MT; Khan A; Cullen DA; Wang X; Primbs M; Zitolo A; Jaouen F; Strasser P Structural and Reactivity Effects of Secondary Metal Doping into Iron-Nitrogen-Carbon Catalysts for Oxygen Electroreduction. J. Am. Chem. Soc 2023, 145, 14737–14747. [PubMed: 37379566]
79. Choi CH; Lim H-K; Chung MW; Chon G; Sahraie NR; Altin A; Sougrati M-T; Stievano L; Oh HS; Park ES; Luo F; Strasser P; Dražić G; Mayrhofer KJJ; Kim H; Jaouen F The Achilles' Heel of Iron-Based Catalysts during Oxygen Reduction in an Acidic Medium. Energy Environ. Sci 2018, 11, 3176–3182.

80. Jagadeesh RV; Junge H; Pohl M-M; Radnik J; Brückner A; Beller M Selective Oxidation of Alcohols to Esters Using Heterogeneous Co_3O_4–N@C Catalysts under Mild Conditions. J. Am. Chem. Soc 2013, 135, 10776–10782. [PubMed: 23668302]

81. Wu G; More KL; Johnston CM; Zelenay P High-Performance Electrocatalysts for Oxygen Reduction Derived from Polyaniline, Iron, and Cobalt. Science 2011, 332, 443–447. [PubMed: 21512028]

82. Ferrandon M; Wang X; Kropf AJ; Myers DJ; Wu G; Johnston CM; Zelenay P Stability of Iron Species in Heat-Treated Polyaniline–Iron–Carbon Polymer Electrolyte Fuel Cell Cathode Catalysts. Electrochim. Acta 2013, 110, 282–291.

83. Liu S; Li C; Zachman MJ; Zeng Y; Yu H; Li B; Wang M; Braaten J; Liu J; Meyer HM; Lucero M; Kropf AJ; Alp EE; Gong Q; Shi Q; Feng Z; Xu H; Wang G; Myers DJ; Xie J; Cullen DA; Litster S; Wu G Atomically Dispersed Iron Sites with a Nitrogen–Carbon Coating as Highly Active and Durable Oxygen Reduction Catalysts for Fuel Cells. Nat. Energy 2022, 7, 652–663.

84. Gunnlaugsson HP Spreadsheet Based Analysis of Mössbauer Spectra. Hyperfine Interact. 2016, 237, 1–6.

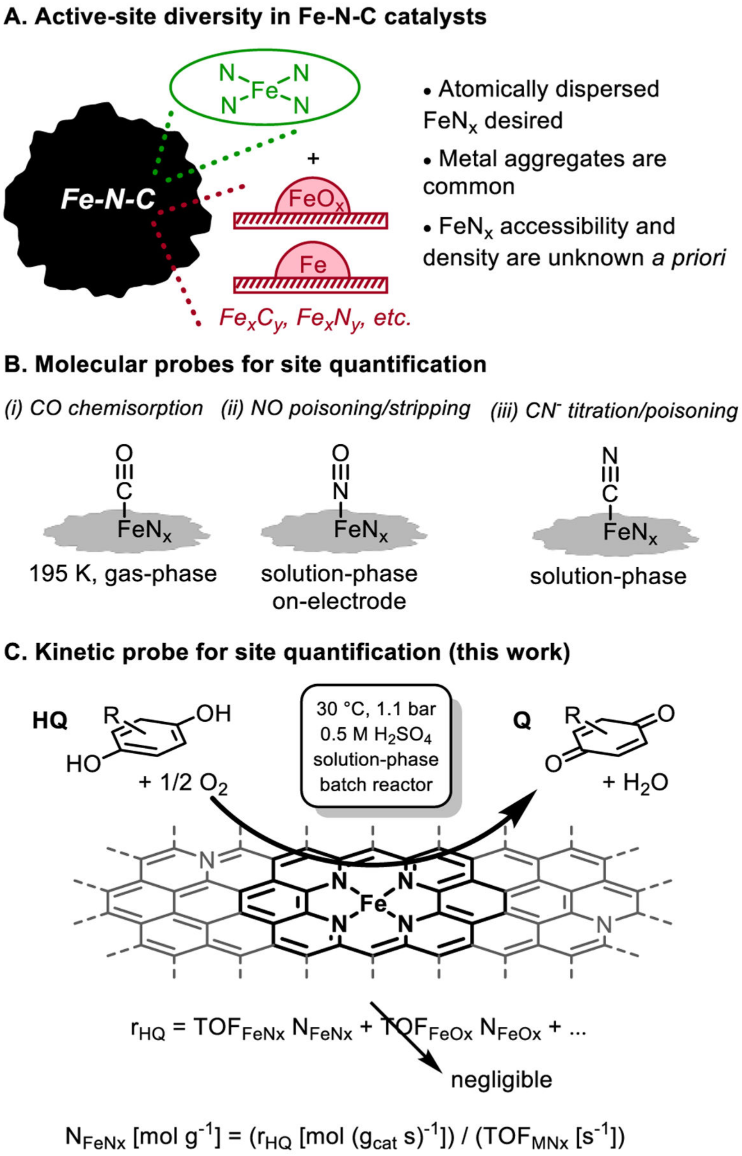

Figure 1.

Comparison of methods to quantify FeN_x site density. (A) Challenges for quantification of catalytically relevant FeN_x sites due to active-site diversity in Fe-N-C catalysts, (B) previously reported molecular probe methods to quantify FeN_x site density, and (C) proposed kinetic probe reaction for FeN_x quantification, where FeN_x are exemplarily illustrated as planar tetrapyridinic FeN_4 sites.

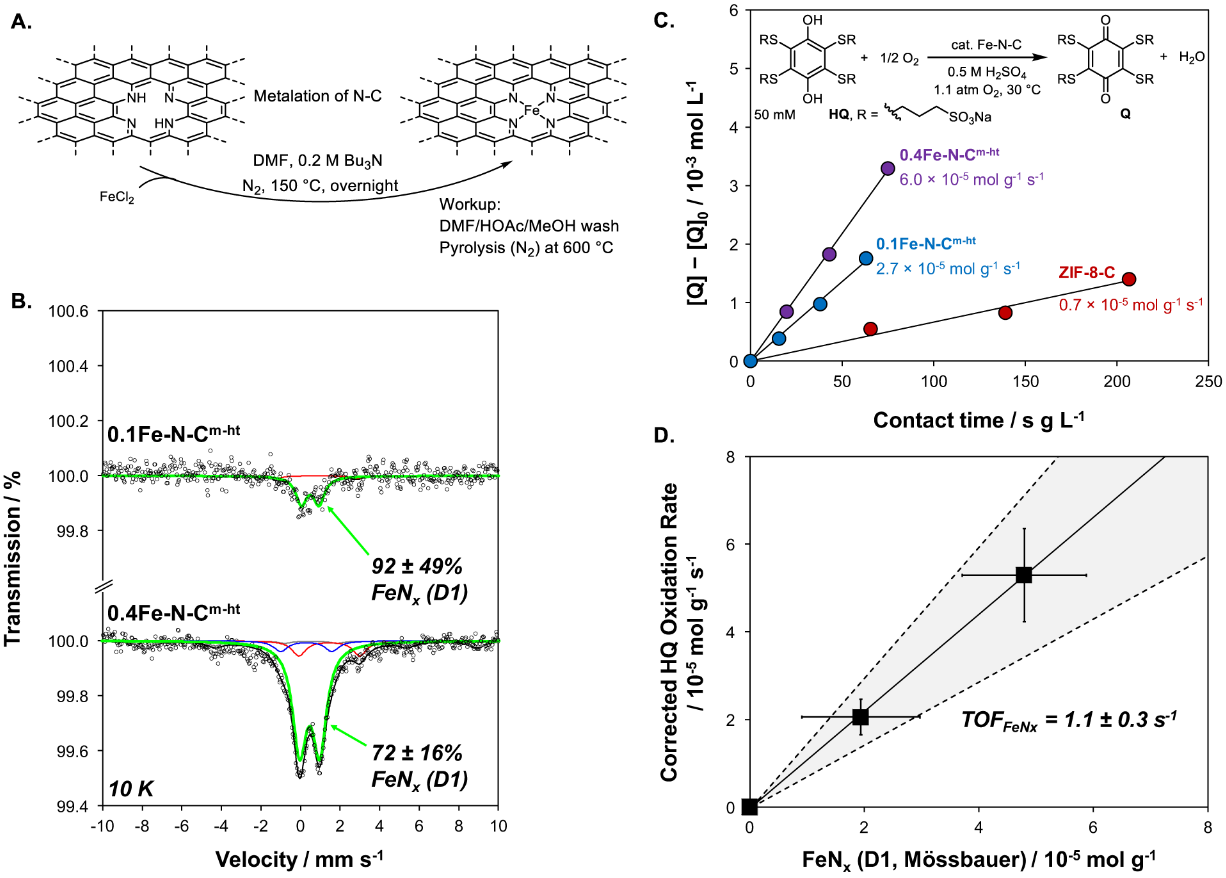

Figure 2.

(A) Preparation of atomically dispersed Fe-N-C catalysts via solution-phase metalation and heat treatment. Planar tetrapyridinic sites are shown as an example. (B) ^{57}Fe Mössbauer spectra (10 K) of 0.1Fe-N-C$^{m\text{-}ht}$ (top) and 0.4Fe-N-C$^{m\text{-}ht}$ (bottom). Data (open points) are fit with a sum (black line) of components assigned to $Fe^{III}N_x$ (D1, green), $Fe^{II}N_x$ (D2, blue), $FeCl_2{\cdot}4H_2O$ (D3, red), and FeO_x clusters (S1, gray). (C) Concentration of quinone formed as a function of contact time on 0.4Fe-N-C$^{m\text{-}ht}$ (purple) and 0.1Fe-N-C$^{m\text{-}ht}$ (blue). The Fe-free analog (ZIF-8-C) is shown in red. Conditions: 30 °C, 1.1 bar O_2, 0.5 M H_2SO_4, $[HQ]_0$ = 50 mM, $[Q]_0$ = 1 mM. Lines reflect regressed fits constrained through the origin. (D) Correlation of the Fe-catalyzed HQ oxidation rate (per $g_{catalyst}$) with the density of FeN_x centers quantified from the Mössbauer spectra in (B) combined with the bulk Fe content measured by ICP-OES, according to eq 1. The corrected rate reflects the difference between the rate measured in (C) and the rate measured on ZIF-8-C, as expressed in eq 2. The solid line reflects the best-fit linear regression to the three data points, where the slope is defined as TOF_{FeNx}. The shaded region bounded by the dashed lines represents the statistical error associated with TOF_{FeNx}.

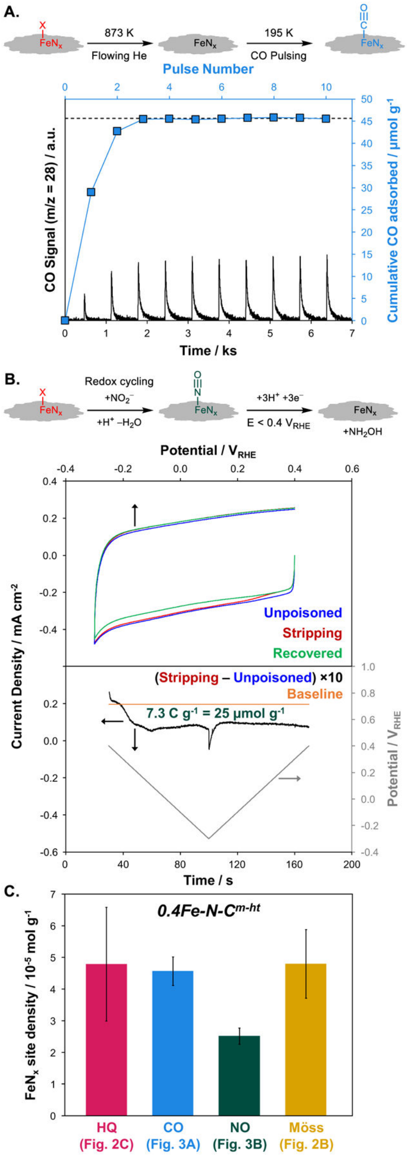

Figure 3.

Probe molecule titrations of FeN_x sites in 0.4Fe-N-C^{m-ht}. (A) CO pulse chemisorption profile (195 K). (B) The upper plot shows cyclic voltammograms measured under Ar-saturated electrolyte (10 mV s^{-1}, 0.5 M acetate buffer pH 5.2) before (blue) and after (red) NO poisoning, and after NO stripping (green), and the lower plot shows the calculated stripping current density ($i_{stripping} - i_{unpoisoned}$) and potential as a function of time derived from the CV measurements. The orange line indicates the integration baseline. See Supporting Information, Section 3.3 for alternative analysis approaches and discussion. (C) Comparison of FeN_x active-site densities obtained by hydroquinone oxidation kinetics (HQ, red), CO pulse chemisorption (CO, blue), electrochemical stripping of NO derived from NO_2^- (NO, green), and ^{57}Fe Mössbauer spectroscopy (Möss, yellow).

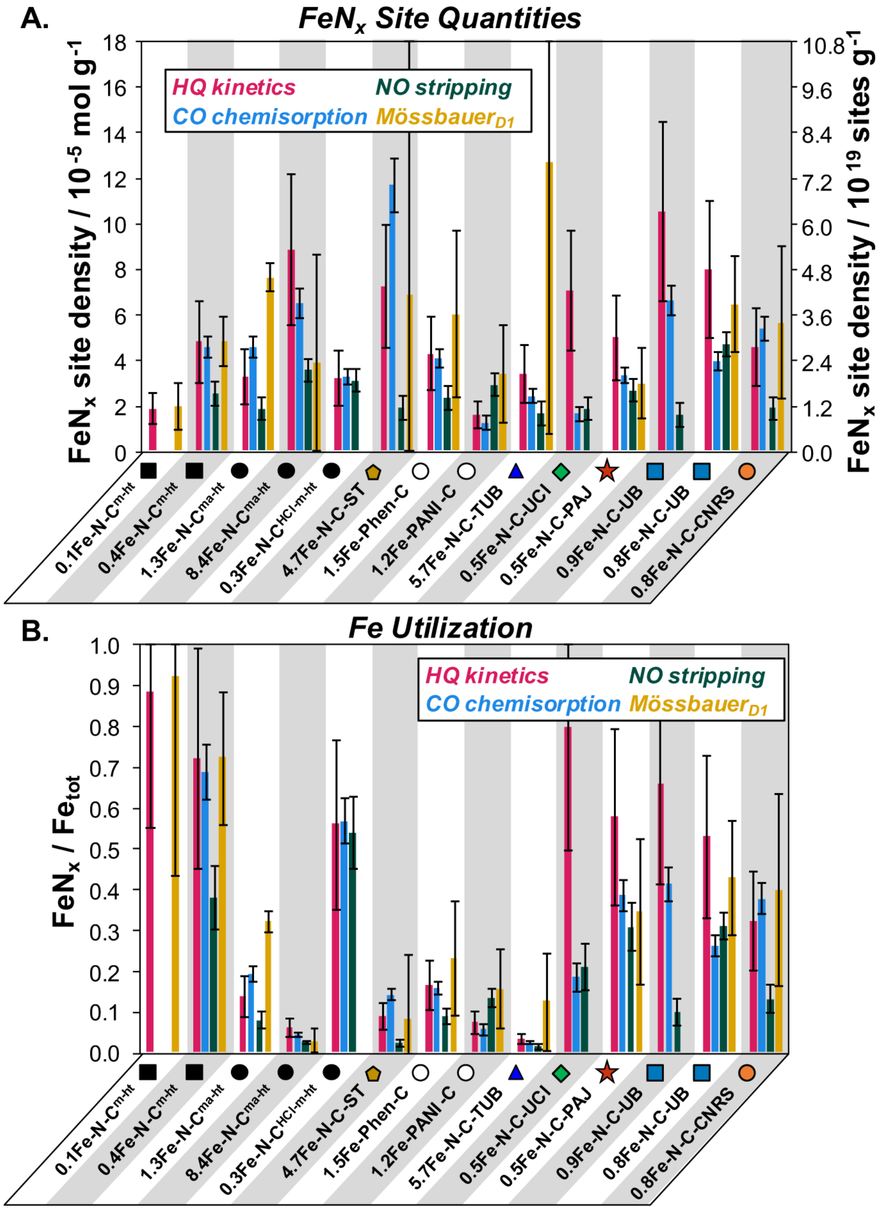

Figure 4.

Comparison of kinetic, spectroscopic, and probe-molecule methods to quantify the density of FeN_x centers in the Fe-N-C catalysts investigated in this work. FeN_x quantities are compared based on (A) a bulk site density basis (mol $g_{catalyst}^{-1}$) and (B) a site utilization basis normalized to the bulk Fe content of each material. Hydroquinone oxidation (red bars), CO pulse chemisorption (blue bars), electrochemical NO stripping (green bars), and ^{57}Fe Mössbauer spectroscopy (yellow bars) are compared. The ^{57}Fe Mössbauer spectra were measured at 10 K on *x*Fe-N-$C^{m\text{-}ht}$ and 1.3Fe-N-$C^{ma\text{-}ht}$ and at 4.2 K for all other reported values. HQ oxidation error bars reflect the propagated standard error of the rate measurement (±20%) and TOF value (±0.3 s^{-1}) used to calculate N_{FeNx}. CO pulse chemisorption error bars reflect the larger of either the error associated with sample mass (±10%) or the error expected from background adsorption determined on an Fe-free ZIF-8-C material (3 μmol g^{-1}, see Figure S12). Electrochemical NO stripping error bars reflect the error derived from control experiments (5 μmol g^{-1}, see section 3.3.2 of the Supporting Information). Mössbauer spectroscopy error bars reflect the statistical error of the least-squares fitting procedure. Alternative analyses based on D1+D2 as the Mössbauer active-site density can be found in Section 6 of the Supporting Information.

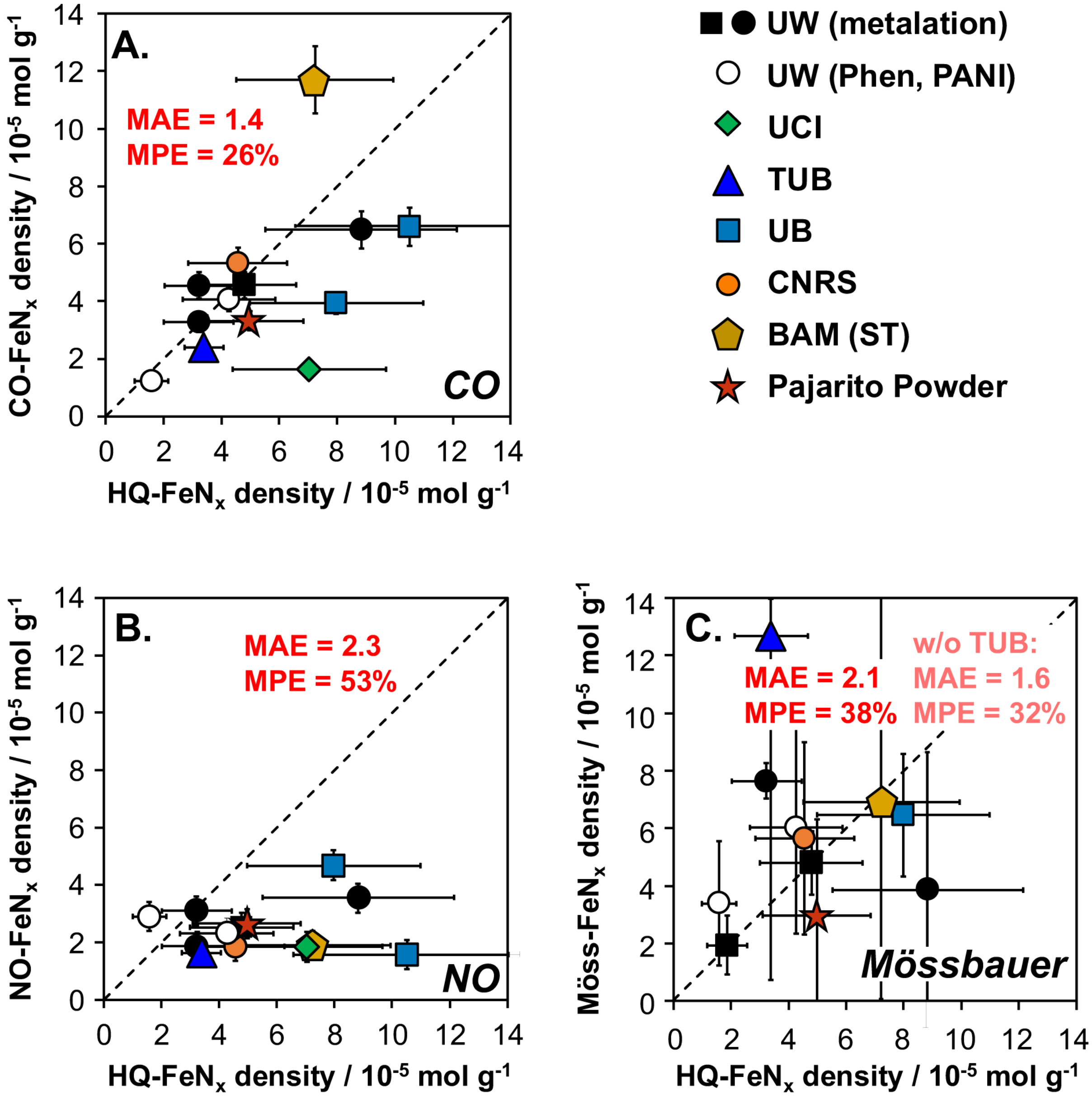

Figure 5.

Parity plots comparing spectroscopic and probe-molecule FeN_x site quantification methods with the kinetic method. The dashed lines indicate equality between the two values. All x-axes reflect kinetically quantified FeN_x site densities derived from hydroquinone oxidation rates and the intrinsic TOF of FeN_x sites ($1.1 \pm 0.3\ s^{-1}$). The y-axes reflect (A) CO pulse chemisorption, and (B) stripping of NO derived from NO_2^-, and (C) Mössbauer spectroscopy. The mean absolute error (MAE) and mean percentage error (MPE) associated with each correlation are calculated according to eq S9 and S10 in the Supporting Information and shown in the plot area. The two xFe-N-C$^{\text{m-ht}}$ materials (black squares) are omitted from the MAE and MPE values in (C) because they were used to estimate TOF_{FeNx} (Figure 2D) and so $N_{FeNx,HQ}$ and $N_{FeNx,Möss}$ are not independently determined.

The MAE and MPE values in (C) without the outlier 5.7Fe-N-C-TUB are reported in pale red text.

Table 1.

Summary of Fe-N-C catalysts investigated in this work.

Fe-N-C catalyst	Bulk Fe Content[a] / wt%	Bulk Fe Content[a] / 10^{-5} mol g^{-1}	Brief Description
0.1Fe-N-$C^{m\text{-}ht}$	0.1	2.1	Solution-phase metalation and heat treatment[13]
0.4Fe-N-$C^{m\text{-}ht}$	0.4	6.6	Solution-phase metalation and heat treatment[13]
1.3Fe-N-$C^{ma\text{-}ht}$	1.3	24	Solution-phase metalation (adventitious air) and heat treatment[13]
8.4Fe-N-$C^{ma\text{-}ht}$	8.4	150	Solution-phase metalation ($Fe(OAc)_2$ precursor, adventitious air) and heat treatment[13]
0.3Fe-N-$C^{HCl\text{-}m\text{-}ht}$	0.3	5.8	Solution-phase metalation of HCl-treated ZIF-8-C and heat treatment[13]
4.7Fe-N-C-ST	4.7	84	Eutectic salt melt metalation and heat treatment[57]
1.5Fe-Phen-C	1.5	26	Pyrolysis of C-supported $[Fe(Phen)_3]^{2+}$[13]
1.2Fe-PANI-C	1.2	22	Pyrolysis of C-supported Fe/polyaniline[13]
5.7Fe-N-C-TUB	5.7	102	Pyrolysis of C-supported Fe/polyaniline[58]
0.5Fe-N-C-UCI	0.5	8.9	Sacrificial support method (SSM)[59,60]
0.5Fe-N-C-PAJ	0.5	8.6	SSM – manufactured by Pajarito Powder[61]
0.9Fe-N-C-UB	0.9	16	Pyrolysis of Fe_2O_3@ZIF-8 composite in 10% H_2/Ar[62]
0.8Fe-N-C-UB	0.8	15	Pyrolysis of Fe_2O_3@ZIF-8 composite in Ar[62]
0.8Fe-N-C-CNRS	0.8	14	Pyrolysis of ZIF-8 mixed with $Fe(OAc)_2$ and 1,10-phenanthroline in Ar at 1323 K[8]

[a] Quantified by ICP-OES.[56]

Table 2.

Qualitative Comparison of FeN_x Active-Site Quantification Methods in this Study.

	Mössbauer spectroscopy	**CO pulse chemisorption**	**Stripping of NO derived from NO_2^-**	**HQ oxidation kinetics**
Pretreatment conditions	Vacuum-ambient pressure, ≤10 K	873 K, flowing He	Nafion film, aqueous acetate buffer (pH 5.2), potential cycling (1.0 to 0.3 V_{RHE}) under Ar and O_2	None
Measurement conditions	Vacuum-ambient pressure, ≤10 K	195 K, flowing He, CO pulsing	Aqueous acetate buffer (pH 5.2), NO_2^- adsorption followed by conversion to NO, stripping from 0.4 to −0.3 V_{RHE}	Stirred slurry, 303 K, 0.5 M H_2SO_4, 50 mM HQ, 1 atm O_2
Fundamental Challenges	• Struggles to differentiate FeN_x from very small FeO_x clusters • Large errors when FeN_x is a minor species	• High-T pretreatment can influence active-site distribution • Measurement conditions are very different from catalytic conditions	• Reproducibility of baseline • Potential cycling pretreatment can influence active-site distribution • Ionomer film may influence site accessibility	• Overcounts if rate of Fe-free analog is not quantified • Inaccurate if FeN_x structural variations impact HQ oxidation TOF
Practical Challenges	• Costly instrumentation • Not broadly available • Long acquisition times (days) and high sample quantities or costly ^{57}Fe precursors	• Costly instrumentation • Requires gas-phase characterization expertise • Medium throughput (~2–3 analyses per day)	• Inexpensive • Requires electrochemical expertise • Medium throughput (~1–2 analyses per day)	• Inexpensive • Requires no specialized equipment • Parallelizable for high throughput
Generality for other MN_x	Mössbauer-active elements are very limited (e.g., ^{57}Fe, ^{119}Sn)	Fe, Sn, Co, Mn reported,[33,75] but CO does not adsorb to NiN_x;[58] others are untested	Reported for Fe, Co, Ni, Sn, Sb, Bi, and Mn,[34,55,76] but only extensively validated for Fe	Untested; requires accurate TOF_{MN_x} determination for each new M and intrinsic reactivity that is above N-C